University of Concepcion
Faculty of Physical Sciences and Mathematics
Geophysics Department

Interaction between historical earthquakes in the seismic gap of Central Chile and the Marga-Marga crustal Fault: The seismic potential of the Valparaiso region

By Javiera Álvarez Vargas

Thesis submitted to Faculty of Physical Sciences and Mathematics to be eligible for the degree of Master of Sciences in Geophysics

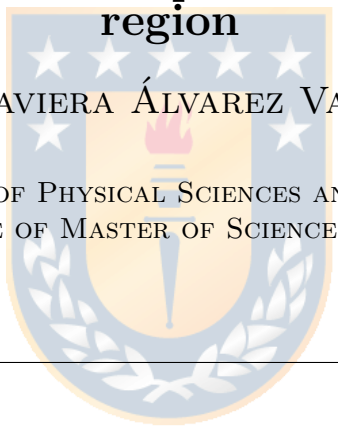

Thesis supervisor:

Dra. María ignacia Calisto Burgos

Committee members:

Dr. Claudio Faccenna - Dr. Joaquín Cortés Aranda - Dr. Rodolfo Araya Durán

June 25, 2025

Concepcion, Chile.

To Irma Velásquez.

Agradecimientos

Quisiera expresar mi más profundo agradecimiento a mis asesores, quienes han sido fundamentales a lo largo de este camino. A Ignacia Calisto, gracias por tus enseñanzas no solo durante mi carrera universitaria, sino también por tu cuidado y protección fraternal. Eres una profesora y profesional excepcional a quien admiro profundamente. Claudio Faccenna, gracias por tus consejos y apoyo incondicional, aun cuando estábamos a miles de kilómetros de distancia y este tema era nuevo para ti, siempre estuviste ahí, guiándome y ofreciendo nuevas oportunidades, enseñándome cómo crecer como investigadora y cómo construir mi carrera en ciencia. Rodolfo Araya, tu conocimiento en modelación durante el curso de métodos matemáticos en el programa de magister en geofísica me ayudó a entender que quería seguir creciendo en esta área, y por esa razón quise hacerte parte de este trabajo. Joaquín Cortés, a pesar de tu tiempo limitado, te sumergiste en este proyecto y brindaste sabios consejos que fueron cruciales para el mejor desarrollo de mi tesis. También extiendo mi agradecimiento a todos los miembros del cuerpo académico del departamento de Geofísica de la Universidad de Concepción, especialmente a Catalina Morales, Carolina Parada, Carla Espinoza, Roxana Encina, y Claudio Carilao, por crear un ambiente académico tan acogedor, y por su constante apoyo. También a la Sra. Alejandra por sus buenos consejos durante los cafecitos y a Don Marco Hernandez por su cariño y soporte durante las ayudantías que me tocó realizar.

A mi familia, Gricel Vargas, Orfelio Vargas, Juan Pablo Álvarez, Gladis González, y Juan Álvarez, gracias por su protección y aliento para perseguir mis sueños, aun cuando significaba estar lejos de casa. Siempre con humildad, respeto y compromiso. Son lo más importante en mi vida.

Dedico esta tesis y mi carrera profesional a mi madre Irma Velásquez. Aunque no pudo estar físicamente presente para el término de mis estudios como siempre habíamos planeado, permanece para siempre en mi corazón, y continúa inspirando mi crecimiento desde el cielo. También dedico este trabajo a la memoria amorosa de Javier Vargas y Byron Javier, cuya presencia llevo conmigo siempre.

A mis amigas de toda la vida Javiera Arias, Valentina Catalán, María José Barría, Belén Álvarez, y Natalia Galindo, y a mis queridos compañeros y amigos de Universidad, Pablo Urra, Fernando Valenzuela, José Carter, y Camila Pincheira. Gracias por su compañía en momentos donde la vida se ponía complicada.

Agradecimientos especiales al Dr. Daniel Stewart por proporcionar los datos históricos esenciales para restringir los procesos estocásticos, a Rodrigo Cifuentes por ser parte del manuscrito, y al Dr. Juan González por sus valiosos conocimientos sobre la falla Marga-Marga.

Esta investigación fue apoyada por ANID-Chile a través del proyecto FONDECYT No. 11180854, "Caracterización de fuentes para tsunamis históricos del Centro-Sur de Chile" dirigido por Ignacia Calisto; por ANID-Chile a través del Centro de Modelamiento Matemático (FB210005) del Programa PIA: Concurso Apoyo a Centros Científicos y Tecnológicos de Excelencia con Financiamiento Basal, y Fondecyt Regular No. 1211649 por Rodolfo Araya; y por el Centro de Investigación Alemán GFZ para Geociencias a través del acceso a instalaciones computacionales y bases de datos durante la estadía del autor en Potsdam, Alemania, 2024.

Acknowledgements

I would like to express my deepest gratitude to my advisors, who have been instrumental throughout this journey. To Ignacia Calisto, thank you for your teachings not only throughout my university career, but also for your fraternal care and protection. You are an exceptional professor and professional whom I deeply admire. Claudio Faccenna, thank you for your advice and unconditional support, even when we were thousands of kilometers apart and this topic was new to you, you were always there, guiding me and offering new opportunities, teaching me how to grow as a researcher, and how to build my career in science. Rodolfo Araya, your knowledge in modeling during the mathematical methods course in the geophysics master's program helped me understand that I wanted to continue growing in this area, and for that reason I wanted to make you part of this work. Joaquín Cortés, despite your limited time, you immersed yourself in this project and provided wise advice that was crucial for the better development of my thesis. I also extend my appreciation to all faculty members of the Geophysics department of University of Concepción, especially to Catalina Morales, Carolina Parada, Carla Espinoza, Roxana Encina, and Claudio Carilao, for creating such a welcoming academic environment, and for your constant support. Also to Ms. Alejandra for her wise advice over coffee and to Mr. Marco Hernandez for his affection and support during my teaching assistant duties.

To my family, Gricel Vargas, Orfelio Vargas, Juan Pablo Álvarez, Gladis Gonzalez, and Juan Álvarez, Thank you for your protection and encouragement to pursue my dreams, even when it meant being far from home. Always with humility, respect, and commitment. You are the most important thing in my life.

I dedicate this thesis and my professional career to my mother Irma Velásquez. Although she couldn't be physically present to witness the completion of my studies as we had always planned, she remains forever in my heart, continuing to inspire my growth from heaven. I also dedicate this work to the loving memory of Javier Vargas and Byron Javier, whose presence I carry with me always.

To my lifelong friends Javiera Arias, Valentina Catalán, Maria José Barría, Belén Álvarez, and Natalia Galindo, and my dear university companions Pablo Urra, Fernando Valenzuela, José Carter, and Camila Pincheira. Thank you for your companionship.

Special thanks to Dr. Daniel Stewart for providing the historical data essential to constrain the stochastic processes, Rodrigo Cifuentes for be part of the manuscript, and Dr. Juan Gonzalez for your valuable knowledges on the Marga-Marga fault.

This research was supported by ANID-Chile through FONDECYT project No. 11180854, "Source characterization for historical tsunamis of Central-Southern Chile" directed by Ignacia Calisto; by ANID-Chile through the Centro de Modelamiento Matemático (FB210005) of the PIA Program: Concurso Apoyo a Centros Científicos y Tecnológicos de Excelencia con Financiamiento Basal, and Fondecyt Regular No. 1211649 by Rodolfo Araya; and by the GFZ German Research Centre for Geosciences through access to computational facilities and databases during the author's stay in Potsdam in 2024.

Abstract

The spatial distribution of earthquake ruptures along seismic segments is crucial for understanding the megathrust cycle in subduction zones. In central Chile, the segment between 32° and 34°S presents a concerning case: despite experiencing several moderate historical earthquakes, it has been identified as a seismic gap since the major 1730 event, which stands as the largest known earthquake in the region.

While subduction processes dominate plate convergence in this region, the role of continental crustal deformation adds another layer of complexity. Of particular interest is the Marga-Marga crustal fault, which runs beneath one of Viña del Mar's most populated areas.

Our research investigates the complex and poorly studied seismic history of this segment by estimating slip distributions and magnitudes for three significant events: the 1730, 1906 Valparaiso, and 1985 Algarrobo earthquakes. We selected these specific events because the 1906 and 1985 earthquakes share similar deformation patterns surrounding the fault trace, which may indicate specific activation mechanisms. Additionally, as we anticipate a future event with similar characteristics to the 1730 earthquake–for which no detailed fault response data exists–modeling this historical scenario provides valuable insights for future earthquake interactions. We combined historical data on vertical displacements and tsunami inundations with a stochastic approach using the logic-tree method. To enhance the reliability of our findings, we developed an uncertainty analysis framework that integrates clustering analysis of maximum slip locations with mean square error calculations, providing a robust assessment of historical earthquake characteristics.

Through Coulomb stress analysis using our preferred slip distributions, we found that historical subduction earthquakes could have triggered fault activation, a significant consideration since crustal earthquakes can produce more concentrated damage than subduction events of similar magnitude.

This comprehensive study lays the groundwork for more detailed investigations of seismic hazard in this densely populated region, particularly regarding the complex interaction between megathrust events and the Marga-Marga fault system. Our findings emphasize the need for further research to better understand the fault response to large subduction earthquakes.

Contents

List of Figures

List of Tables

Chapter 1

Introduction

Subduction zones have been the subject of numerous studies since the advent of plate tectonics. These zones, formed by convergent plate boundaries, where one plate slides under another due to ridge-push and slab-pull forces (Spence (1987)), lead to crustal thickening and thus to an orogenesis process. These forces largely determine how plates move and consequently determine how stresses accumulate in those segments (Spence (1987)), resulting in volcanic eruptions, seismic activity, and the transport of minerals into the mantle (Zheng and Zhao (2017)). In the case of Chile, subduction occurs when the Nazca plate slides below the Sudamerican plate. This interaction, has provided a large register of historical earthquakes, making the subduction zone of Chile an ideal laboratory for investigate the seismic cycle (Beck et al. (1998)).

The Chilean segment of subduction Nazca-Sudamerican plate, has been the scene of megathrust earthquakes with moment magnitudes (Mw) greater than 8.5, such as Mw 9.5 1960 Valdivia earthquake and Mw 8.8 2010 Maule earthquake, with periods of recurrence of tens to hundreds of years (Cisternas et al. (2005); Moreno et al. (2012)). The slip distribution caused by this type of events, is heterogeneous in terms of strength or frictional characteristics of the fault zone material (Weng and Ampuero (2019)). Reconstructing these slip patterns for historical events requires integrating multiple datasets, including geological evidence such as coseismic uplift, tsunami records, and historical accounts, often analyzed through probabilistic approaches to account for uncertainties. These heterogeneities are related to the asperities, and the barriers to earthquakes limits, which control the release of seismic moment and rupture area during earthquakes. An asperity concentrates the release of energy and slip distribution in rupture zones, while barriers trigger little to no slip, acting, as their name implies, as barriers to earthquake rupture. The seismic impact is not limited exclusively to megathrust earthquakes, but also comes from the potential for triggering crustal fault events affecting geological structures below the ground. The spatial patterns of slip distribution and stress release during these events directly influence how stress is transferred to surrounding geological structures, including crustal faults in the overriding plate.

The occurrence of significant seismic events has not only affected Chile, but also other subduction zones around the world. For example, we have the massive 9.2 magnitude earthquake in Alaska in 1964 (Suito and Freymueller (2009)), as well as the Mw 9.0 magnitude earthquake in Japan during the Tohoku-Oki event (Simons et al. (2011)). These events share similarities with the 2010 Maule earthquake in Chile. What is intriguing about these seismic events, is their commonality: they all involve thrust events along subduction zone plate interfaces. The noteworthy aspect of these events is how they act as triggers for potentially hazardous earthquakes

(with a magnitude greater than approximately Mw 5.5) within the overriding plate (Gomberg and Sherrod (2014)). The proximity of these triggered earthquakes to populated areas raises concerns about their potential hazard (Santibáñez et al. (2019)). Within subduction zones, normal-fault earthquakes are commonly understood as manifestations of the downward deflection and descent of oceanic plates at convergent plate boundaries. These earthquakes, characterized by shallow normal-fault mechanisms behind the trench and above the subducting slab, are crustal in nature (Choy and Kirby (2004)). They are particularly generated by geological structures such as crustal faults that enhance this type of seismicity and arise as the overriding plate adjusts to the collision with the buoyant oceanic lithosphere. These triggered earthquakes, although smaller, may pose a greater hazard than the massive subduction thrust events themselves, especially when occurring near densely populated regions (Choy and Kirby (2004)).

Crustal faults, usually have seismicity with longer recurrences (thousand of years) than those of subduction, at shallow depths up to 30 km within the overriding South American plate, and generate earthquakes with maximum magnitudes of Mw 7.0-7.5 (e.g., Barrientos et al., 2004; Leyton et al., 2010; Jara-Muñoz et al., 2017; Cortés-Aranda et al., 2022). Subduction earthquakes are considered the principal seismic hazard in Chile, because of their potential to generate significant damage in the country and and higher frequency. However, crustal earthquakes, can be more destructive at the local level because of their lower hypocentral depth, despite occurring less frequently (Santibáñez et al. (2019)). Therefore, given their greater destructive potential, it is crucial to not overlook crustal events, acknowledging that in nature, these events exhibit different behaviors depending on factors such as fault orientation, stress state, and position within the seismic cycle. The timing of stress transfer throughout the seismic cycle, including interseismic periods, is particularly interesting, as faults may respond differently to stress perturbations depending on their accumulated stress and proximity to failure.

These two types of events, are currently a great potential seismic hazard for the Valparaiso region in Central Chile, specifically for the city of Viña del Mar, where the Marga-Marga fault is located. Historical observations indicate deformation along the Marga-Marga fault coinciding with megathrust earthquakes, which is especially concerning since this area is currently recognized as a seismic gap.

This research aims to assess the potential for subduction earthquakes in Central Chile to trigger stress transmission and reactivate the crutal fault. The approach will involve reconstructing slip distributions of the 1730, 1906, and 1985 historical earthquakes using geological and historical data (including coseismic uplift and tsunami records) combined with logic tree methodologies to address uncertainties, and subsequently evaluating Coulomb Failure Stress changes between these reconstructed events and the Marga-Marga crustal fault. The study will then simulate the potential reactivation of the fault and its potential impact on the surrounding area. It is important to note that this study does not definitively confirm a reactivation of the Marga-Marga fault, but rather seeks to evaluate its behavior in response to large subduction events in the scenario of a possible reactivation.

1.1 Hypothesis

The Valparaíso region in central Chile represents a critical seismic gap with significant accumulated strain since the 1730 earthquake. This research addresses two interconnected objectives: first, the systematic reconstruction of slip distributions from major historical earthquakes in central Chile, which provides essential insights into rupture processes and seismic behavior patterns; and second, the evaluation of stress transfer mechanisms between these subduction events and the Marga-Marga crustal fault beneath Viña del Mar.

Understanding historical earthquake characteristics through detailed slip modeling is fundamental for seismic hazard assessment, while the potential triggering of crustal faults adds another critical dimension to regional evaluation. Historical observations suggest correlations between major earthquakes and localized damage patterns along the Marga-Marga fault, yet the mechanical relationships governing such interactions remain unquantified. The following research questions guide this investigation:

- Can subduction earthquakes on the Valparaiso segment trigger the Marga-Marga Fault?
- Which historical events need to be investigated to prove fault activity?
- How does the geology of the sector impact the interaction between the fault zone and subduction megathrust earthquakes? Does the fault works as an exacerbating factor or as a protective barrier?

"The reconstruction of historical earthquakes in central Chile provides insights into the rupture processes of shallow and deep seismic events. These patterns reveal historical seismic activity and explore potential interactions between seismic events and the Marga-Marga Fault, identifying it as a key area of lithological weakness that could influence future seismic behavior."

1.1.1 Objectives

To address these research questions, this study pursues a dual approach that combines earthquake source characterization with fault interaction analysis. The investigation is structured around the following objectives:

General objective:

Characterize historical earthquake rupture processes in central Chile and assess the conditions under which these subduction earthquakes are more likely to trigger stress transmission to the Marga-Marga crustal fault.

Specific objectives:

1. Determine and characterize the slip distribution patterns of historical tsunamigenic earthquakes in Central Chile, including uncertainty analysis of rupture parameters.
2. Stablish Coulomb stress changes induced by the reconstructed historical earthquakes on the Marga-Marga fault system, in order to identify the rupture characteristics that maximize fault reactivation potential.

Chapter 2

Manuscript

Megathrust earthquake characterization along the central Chile Gap: Exploring Historical Earthquakes Using the Stochastic Logic Tree Approach

Javiera Álvarez[1], Ignacia Calisto[1], Claudio Faccenna[2], Rodrigo Cifuentes-Lobos [3], Joaquín Cortés[4] and Rodolfo Araya[5]

[1]Department of Geophysics, University of Concepcion, Concepcion, Chile
[2]GFZ German Research Centre for Geosciences Wissenschaftpark "Albert Einstein", Potsdam, Germany
[3]Faculty of Mathematics, Informatics and Natural Sciences Department of Mathematics, Universität Hamburg, Germany
[4]Department of Earth Sciences, University of Concepcion, Víctor Lamas 1290, Concepcion, Chile
[5]Department of Mathematical Engineering & CI2MA, University of Concepcion, Concepción, Chile

Key Points:

- Reconstruction of historical interplate seismicity in central Chile 32°-34°S
- Logic tree approach as a method for stochastic model generation
- Distribution of slip and rupture patterns for the 1730, 1906, and 1985 megathrust earthquakes.

Abstract

The spatial distribution of earthquake ruptures is crucial for understanding megathrust cycles in subduction zones. Despite experiencing several historical earthquakes, the segment from 32° to 34°S in Chile is recognized as a seismic gap, having not experienced an event comparable to the 1730 earthquake in nearly 300 years.

Our research quantifies slip distributions and magnitudes for three major seismic events in central Chile: the 1730, 1906, and 1985 earthquakes. Using a stochastic logic-tree approach constrained by historical data, we determined that the 1730 event ruptured in a large patch nearly 1000 km with an estimated magnitude of Mw 9.1, primarily affecting the shallow portion of the subduction zone. In contrast, the 1906 earthquake (Mw 8.1) ruptured approximately 600 km, with the main slip concentrated along a 200 km section in deeper portions of the subduction zone. Similarly, the 1985 event (Mw 8.0) ruptured about 373 km total, with a primary slip zone of 170 km at depths comparable to the 1906 earthquake.

This detailed slip reconstruction reveals systematic depth-dependent rupture patterns that influence regional stress transfer mechanisms. Quantitative characterization provides valuable constraints for understanding mechanical coupling between subduction processes and crustal response, advancing our ability to assess seismic potential in this densely populated region.

Plain Language Summary

Understanding where and how historical earthquakes occur is essential for studying seismic activity, focusing on central Chile, a region with a long history of earthquakes. Although smaller earthquakes, such as those in 1822, 1906, 1985, and 2017, have occurred between 32° and 34°S, no major event comparable to the 1730 earthquake has occurred in nearly 300 years, raising questions about the potential for another large earthquake.

In this study, we examined three significant earthquakes in central Chile: the 1730, 1906, and 1985 events. Using historical data and modeling techniques, we estimate ground displacement, rupture lengths, and magnitudes for each earthquake. We found that the 1730 event had a rupture length of about 1000 kilometers and a magnitude of approximately 9.1. The 1906 and 1985 events were smaller, with rupture lengths of nearly 600 and 373 kilometers and magnitudes of 8.1 and 8.0, respectively. These results offer valuable insights into the seismic behavior of central Chile.

2.1 Introduction

Subduction zones, formed at convergent plate boundaries through ridge-push and slab-pull forces (Spence (1987)), generate Earth's largest earthquakes and drive significant geological processes, including orogenesis, volcanism, and deep mineral transport (Rikitake (1976); Zheng and Zhao (2017)). The most notable megathrust events include the 1960 M_w 9.5 Chile (Cisternas et al. (2005)), 1964 M_w 9.2 Alaska (Johnson et al. (1996)), 2004 M_w 9.2 Sumatra-Andaman (Tanioka et al. (2006)), and 2011 M_w 9.0 Tohoku-Oki (Simons et al. (2011)) earthquakes. The Chilean subduction zone, where the Nazca Plate descends beneath the South American Plate, stands out as a natural laboratory for researching the seismic cycle (Beck et al. (1998)).

Along this margin, recurring large historical and prehistoric earthquakes (Stewart (2019)) demonstrate heterogeneous rupture patterns that reflect variations in interface coupling, characterized by segments that repeatedly host high slip (asperities) separated by regions that act

as persistent barriers to rupture propagation, as observed in many subduction zones worldwide (Philibosian and Meltzner (2020)). This segmentation fundamentally influences rupture extent and energy release patterns during major events.

Central Chile exhibits a complex history of accumulation and release of strains. The 2010 Maule earthquake (M_w 8.8) exemplified the seismic potential of identified seismic gaps along the subduction interface (Moreno et al. (2012)). These seismic gaps, are characterized by prolonged periods without significant strain release (Ruegg et al. (2009)). Following this event, attention has turned to another seismic gap, bounded by the rupture zones of the 2010 Maule and 2015 Illapel earthquakes (Satake and Heidarzadeh (2017); Carvajal et al. (2019)) in the Valparaiso segment (32°-34°S) (Figure 2.1). Although this portion has experienced moderate seismic activity, including for example the 1985 M_w 8.0 and more recently the 2017 M_w 6.9 event (Bravo et al. (2019); Ruiz and Madariaga (2018)), these ruptures have not fully dissipated the accumulated strain since the last major event in 1730 (M_w 9.0) (Carvajal et al. (2017)).

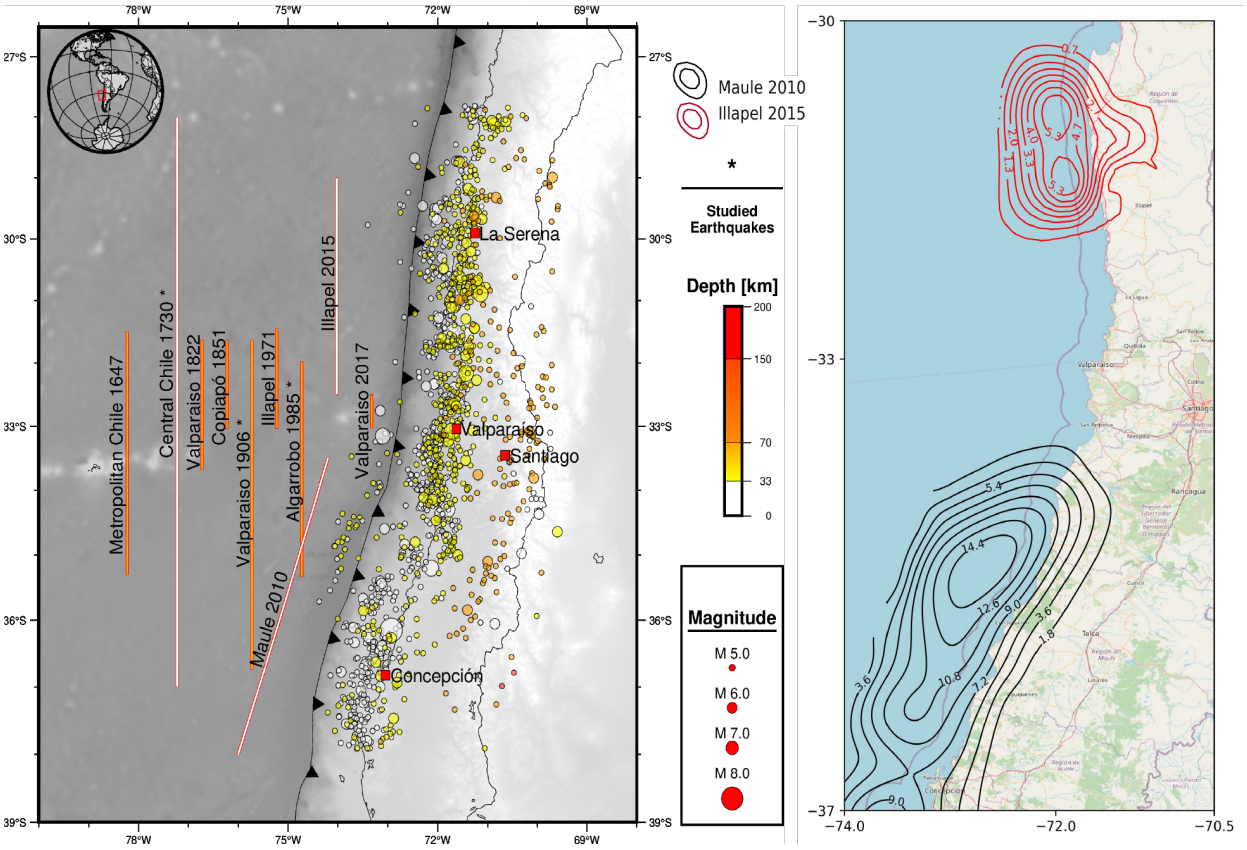

Figure 2.1: Panel a) Historical Earthquakes and Seismicity of South-central Chile: The seismicity in this panel is classified based on earthquakes with a magnitude of 5 or higher, occurring between January, 1973 and December, 2023 (Barrientos and Team (2018)). The white lines represent extensive and shallow rupture areas along the coast, while the yellow lines indicate minor and deeper ruptures that directly affected the Valparaiso region. Panel b) Slip Distributions of the Maule 2010 Earthquake and Illapel 2015 (Moreno et al. (2010); Tilmann et al. (2016)): These two earthquakes delimited the gap area of the Valparaiso region in Chile.

To analyze the seismic history of the main area, we applied the Logic Tree method (LT), a technique widely used in seismic hazard analysis for future earthquakes and tsunamis (e.g.., Cifuentes-Lobos et al., 2023; Fukutani et al., 2018; Goda and Song, 2016), as well as to reconstruct the seismic memory of past events (San Martín et al. (2024)). Our study focuses on the region between 27°S and 39°S, where we examined the slip distributions of 1730, 1906, and 1985 earthquakes presented in Figure 2.1a.

By incorporating rupture parameters, fault geometry, and historical context, we used a numerical model (e.g., LeVeque et al., 2017) to generate multiple seismic scenarios. These scenarios were further constrained using vertical displacement data and tsunami records and analyzed using statistical methods to reduce uncertainty, allowing us to generate realistic and heterogeneous models for each seismic event.

Our research highlights the significant impact of 1730, 1906, and 1985 historical seismic events in the Valparaíso region. The 1730 earthquake had an estimated rupture length of 1000 km and a magnitude exceeding M_w 9.0. The maximum slip occurred at shallow depths (within 20 km from the trench). This condition allows for the production of more tsunamigenic earthquakes in this segment. This new information on the slip pattern is compatible with the recorded damage along the Chilean coast and resulted in tsunamis with wave heights of 10 meters in the segment (Carrasco et al. (2016); Carvajal et al. (2017); Stewart (2019)).

In contrast, the 1906 and 1985 earthquakes ($M_w \sim$ 8.0-8.2) had moderate rupture lengths between 300-600 km. Unlike the 1730 event, these earthquakes concentrated their significant slip in much smaller main patches (approximately 200 km), despite their considerable total rupture zones. The maximum slip for these events was observed in deeper segments ($\sim$ 40 km from the trench), with the 1906 event rupturing near the coast of Algarrobo at 33.5°S, and the 1985 event occurring between Concepción and Los Vilos. Both events caused coastal uplift, strong shaking, and structural damage. Minor tsunamis were reported, with run-up heights not exceeding 3 meters (Palacios Roa (2016); Carrasco et al. (2016); Stewart (2019); Carvajal et al. (2019)).

Our findings suggest that the ruptures of these two events occurred in the deepest part of the seismogenic zone, consistent with our slip reconstructions and previous analyses by Carvajal et al. (2019). Following Bilek and Lay (2018), our modeling reveals two primary rupture modes in the central Chilean margin: moderate to large events (Mw 7.8-8.3) predominantly affecting deeper portions of the seismogenic interface with limited tsunami generation, while great earthquakes (Mw $\geq$ 8.5) like the 1730 event can propagate through shallow segments with greater tsunamigenic potential. Our slip distribution analysis indicates that post-1730 earthquakes have mainly ruptured deeper sections of the coupled zone, leaving substantial shallow portions with accumulated strain energy. This spatial segregation of slip suggests elevated potential for a future great earthquake with enhanced tsunami hazard in this densely populated region.

2.2 Tectonic and Seismotectonic setting

The Chilean margin hosts one of Earth's most seismically active subduction zones, where magnitude >8 interplate underthrusting earthquakes have occurred along its entire length (Beck et al. (1998); Pardo et al. (2002)). The central zone of Chile, defined between latitudes 31.5°S and 34.5°S, has experienced several large subduction earthquakes over recent centuries (Moreno et al. (2011)) and represents the most densely populated coastal region of the country.

A fundamental change in the configuration of the subduction zone occurs near 33°S (Valparaiso latitude), marked by variations in volcanic arc activity and continental margin structure coincident with the subduction of the Juan Fernandez Ridge (JFR) (Von Huene et al. (1997); Pardo et al.

(2002)). The JFR subduction correlates with a sharp change in the slab dip and is considered a primary factor that explains the subduction of the flat slab north of 33°S (Cahill and Isacks (1992); Von Huene et al. (1997); Gutscher et al. (2000); Yáñez et al. (2001); Pardo et al. (2002)). At the trench axis, the JFR acts as a barrier to sediment transport, impounding deep trench sediments from the south while leaving minimal sediment to the north. The adjacent continental margin encompasses the Valparaíso basin and a series of shallow forearc basins on the shelf extending southward, while central and southern Chile are characterized by a normal steep-dipping subduction zone (Von Huene et al. (1997)).

This complex tectonic setting is reflected in the region's seismic behavior. The area is bounded by the rupture zones of the 2010 Maule and 2015 Coquimbo Earthquakes (Figure 2.1). Carvajal et al. (2019) identified a bimodal seismogenic behavior in this region, where exceptional tsunamigenic events like the 1730 earthquake alternate temporally with sequences of lower-magnitude, deeper ruptures that pose reduced tsunami threat. Historical seismicity in the region, which spans from 1575 to 2017, shows remarkable variability in rupture modes while maintaining periodic occurrence (Comte et al. (1986); Barrientos (1995)). Analysis by Comte et al. (1986) reveals that great earthquakes in the region differ significantly, with rupture lengths varying by a factor of three. This variability is exemplified by two extreme cases: the 1730 event, the largest reported in the region, and the 1985 earthquake, one of the smallest but best-studied events in the sequence (Lomnitz (1970); Barrientos (1995); Carvajal et al. (2017)).

Table 2.1: Insights into Historical Earthquakes in central Chile

Date	Magnitude	Rupture limit	Depth
July 8, 1730	9.0-9.3M_w (Carrasco et al. (2016); Carvajal et al. (2017))	∼1000 km (27.3° - 36.6°S) (Carrasco et al. (2016))	∼15 km (Carvajal et al. (2014))
August 16, 1906	8.2M_w (Christensen and Ruff (1986))	500 km (31.7°-31.1°S) (Carvajal et al. (2019))	40 km (Okal (2005))
March 3, 1985	8.0M_w (Comte et al. (1986))	170 km (32.7°-34°S) (Comte et al. (1986))	40 km (Christensen and Ruff (1986))

The historical record suggests that smaller events (e.g., 1822, 1906) primarily ruptured deeper portions of the fault plane (Carvajal et al. (2019)). This pattern raises important questions about the potential for future large earthquakes, particularly given that no event comparable to the 1730 earthquake has occurred in nearly three centuries.

2.3 Materials and Methods

We develop a comprehensive methodology grounded in a historical seismicity research in central Chile. The research specifically focuses on this portion, taking into consideration the potential for a near-future event that could release the seismic gap imposed by the 1730 earthquake (Carvajal et al. (2017)). Our methodology combines the collection of historical seismic data, stochastic generation of rupture scenarios, constraint processes, and validation of resulting models, illustrated in Figure 2.3. Our intention is to reconstruct slip patterns from key historical events, specifically those in 1730, 1906, and 1985, which are crucial for understanding the impacts of subduction events

in the Valparaíso segment. The selection of these events was based on the availability of well-documented historical data regarding vertical displacement and tsunami arrival, as documented by Stewart (2019); Carvajal et al. (2019); Wood et al. (1987); Comte et al. (1986), enabling accurate slip pattern reconstruction.

2.3.1 Reconstructing Historical Rupture Areas Using Logic Tree Approach

The arrangement of subfaults to generate stochastic earthquake scenarios employs a logic tree (LT) structure (Cifuentes-Lobos et al. (2023); LeVeque et al. (2017)). To generate hypothetical rupture scenarios, random slip distributions area created using a combination of fault-defining parameters. The fault is divided into a $n \times m$ matrix of rectangular subfaults, where the dimensions are determined by the number of subfaults along dip, strike, and depth obtained from the Slab2 model (Hayes et al. (2018)), fault length, and its aspect ratio. Following the methodology introduced by (Cifuentes-Lobos et al. (2023)), a particular earthquake can be described by specifying the slip on each subfault, i.e., if we have N subfaults, this forms a vector $s \in \mathbb{R}^N$ where s_i is the slip on the sth subfault in an N-dimensional space. The slip values in this study are modeled using a joint lognormal distribution, which is obtained by exponentiating a Karhunen-Loeve (K-L) expansion (Mai and Beroza (2002); LeVeque et al. (2017)). This expansion is a linear combination of eigenvectors and eigenvalues derived from a covariance matrix, which is influenced by the distribution of subfaults defining the fault geometry. The key parameters in this model are the moment magnitude M_w, the mean slip value for any subfault μ, and the covariance matrix, which describes the slip of one subfault relative to another. The covariance between the slips of subfaults i and j is denoted as $\hat{C}_{ij} = \mathbb{E}[(s_i - \mu_i)(s_j - \mu_j)]$. The K-L expansion aims to represent the slip as a combination of the covariance matrix's eigenvectors.

$$s = \mu + \sum_{k=1}^{N} z_k \sqrt{\lambda_k} \upsilon_k \tag{2.1}$$

where s represents the stochastic process, μ is the mean slip, z_k is the expansion coefficient, and λ_k and υ_k are the eigenvalues and eigenvectors, respectively.

The K-L expansion calculates the moment magnitude M_w by considering the total slip across the entire fault plane and taking into account the rigidity of the rock. For example, if there is an average slip of 10 meters distributed over a fault that is 100 km wide and 1000 km long, the resulting magnitude would be M_w 9. Therefore, we use this average slip as a fixed value. However, if the fault was only 500 km long, the magnitude would be M_w 8.8, and a slip of 20 meters would be necessary for a magnitude 9.0 event (LeVeque et al. (2017)).

2.3.2 Historical Observation and Constrain Process

A multitude of models becomes imperative to address both empirical and random uncertainties, ensuring the diverse nature of slip distributions. This approach, which favors heterogeneous slip distributions (Cifuentes-Lobos et al. (2023)), is superior to their homogeneous counterparts, which tend to underestimate tsunami intensities.

Although LT structures have the capacity to generate an extensive array of random models, not all of them inherently capture the characteristics of natural or plausible earthquakes due to their stochastic nature. To address this, it becomes essential to introduce and enforce restrictions, first using vertical displacement data restrictions and second, tsunami data, to filter out implausible

scenarios as shown in Panel a) in Figure 2.3. The order of the restrictions is important and affects the final result.

Deformation data restrictions

Given a subduction earthquake, the scale of vertical displacement at the surface caused by, it is proportional to the amount of slip of the seismic event. The major displacement is not expected to occur "ahead" of low slip values; rather, higher deformation values measured on the land should be associated with the main slip patches of the earthquake. This, e.g., in the case of central Chile, the highest historical displacement reported should have latitudes similar to the greatest slip amounts of the models.

This constraint eliminates random models whose main slip patches do not fall within a certain tolerance defined by the user and dependent on the earthquake magnitude in front of the highest values of vertical displacement.

This type of restriction can be implemented in two ways: in a qualitative and quantitative form. The qualitative approach is used for historical earthquakes where precise information regarding vertical changes in the ground is not available. However, this constraint can be applied through observations of uplift and subsidence in historical documents, termed as "coincidence constraint". The second method, known as the "magnitude constraint", is utilized when there are exact vertical displacement data in terms of meters of uplift or subsidence in the historical documentation.

Tsunami data restrictions

The constraint based on tsunami data is an iterative process in which the order of operations is crucial. In its basic form, this process consists of the tsunami model and the restrictions based on tsunami data. Taking in considerations the number of data density, we create bands in the models, given them more weight in the restriction process the portion with more tsunami data, defining a penalty for those that have fewer data points.

In this way, for a reference band that contains the largest amount of tsunami data, the slip distribution of the stochastic models in terms of patch and slip quantity will be filtered where the highest tsunami water depth is recorded by tsunami reference points in historical documents such as Udias et al. (2013); Carrasco et al. (2016); Stewart (2019); Carvajal et al. (2019). By default, the methodology discards the $\frac{\rho_i}{\rho_{RB}}\%$ where ρ_i and ρ_{RB} are the data densities of the i-th band and the reference band, respectively. This approach ensures that the remaining models retain high-value slip features in regions where data allow for clear resolution. However, there is an inherent uncertainty when working with historical earthquakes, as historical records are often imprecise, and many instances of tsunami or vertical displacement data were not documented in older archives. This introduces bias in the results; however, by compiling historical research, we can identify which models align more closely with the available historical data.

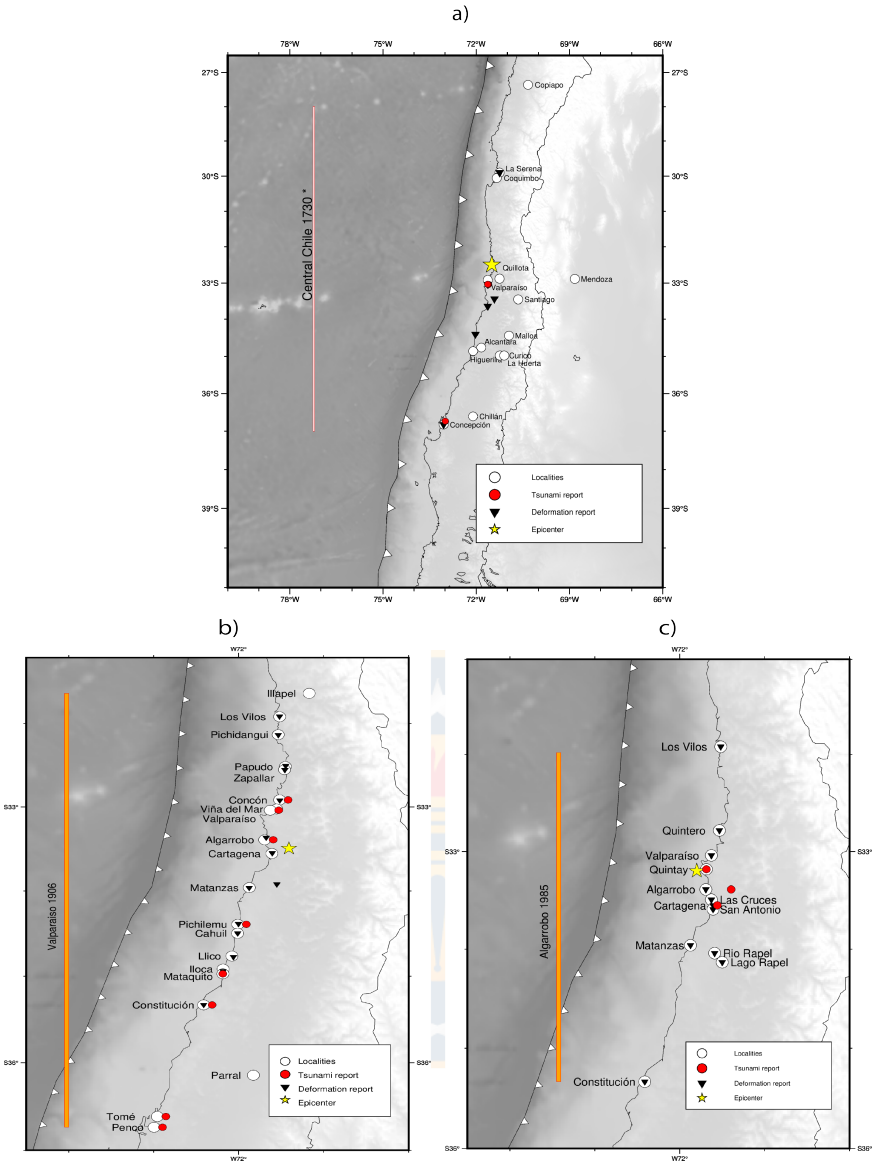

Figure 2.2: Estimated rupture zones and historical evidence for the (a) 1730, (b) 1906, and (c) 1985 earthquakes of central Chile. Each panel shows estimated rupture areas (colored lines) at the same scale by longitude, documented vertical displacement measurements (triangles), tsunami observations (red circles), affected localities (white circles), and proposed epicentral locations (star). Historical data compiled from multiple historical sources (Udias et al. (2013); Carrasco et al. (2016); Carvajal et al. (2017); Stewart (2019); Carvajal et al. (2019); Wood et al. (1987); Comte et al. (1986)).

2.3.3 Seismic Source Modeling and Characterization

When generating the LT approach, different input parameters are combined for each earthquake. Once the constrained models are obtained, the definitive parameters for the most probable source of these earthquakes will indicate the moment magnitude of the results.

To characterize the final slip distributions, the most probable value of the i-th fault is estimated by calculating the slip value that maximizes the probability density function (PDF), ensuring the maximization of probability for each subfault. However, the resulting slip distribution from these

models may not necessarily match the most frequently calculated moment magnitude in the initial estimation. To address this, the slip field is scaled by a multiplicative factor that adjusts the sum of the contribution of each subfault to the desired moment magnitude Mo_{MP}, which is determined by the most probable moment magnitude MP. Therefore, if the resulting magnitude of the characterization is Mo_c, the final slip distribution S_f is obtained by multiplying the characterized slip vector S_c by the ratio between the most probable moment magnitude Mo_{MP} and the moment of the characterized slip vector. By recalculating the new moment of each subfault and summing their contributions, the final moment magnitude of the models is achieved. This can be seen in the following equation:

$$S_f = \frac{Mo_{MP}}{Mo_c} S_c \tag{2.2}$$

2.3.4 Uncertainties associated

The number of qualitative and quantitative data recorded for each seismic event determines the number of models that pass all restriction filters. This leads to the question of which of these models most accurately represents the specific event. To address this, it is crucial to take into account the uncertainties inherent in all models that have gone through the restriction process.

In order to mitigate potential bias, a methodology presented in Figure 2.3 is applied to determine the most representative results for each event. This involves initially clustering the models based on the peak slip values for each sub-fault. The K-means algorithm is used for this clustering (see Panel b) and c) in Figure 2.5), which calculates centroids for each group of maximum slip values, as defined by:

$$Kmeans = \sum_{k=1}^{K} \sum_{x \in C_k} \|x - \mu_k\|^2 \tag{2.3}$$

where K represents each generated cluster, X denotes the number of models, and $\|x - \mu_k\|$ is the Euclidean distance between a point x and its centroid μ_k.

The cluster with the largest number of models is used to compute the mean slip value of the models.

Subsequently, the Mean Squared Error (MSE) is calculated using two terms. The first term is determined by comparing the coordinates of the estimated maximum slip position in each model to the average maximum slip position of the entire cluster. Secondly, the MSE is calculated by comparing the average maximum slip of the entire cluster to the maximum slip of each individual model. Specifically:

$$MSE = \frac{1}{n} \sum_{i=1}^{n} \sqrt{(x_i + \bar{x})^2 + (y_i + \bar{y})^2} \tag{2.4}$$

where (x_i, y_i) are the coordinates of the maximum slip positions i, and $(\bar{x}, \bar{y})$ represent the average positions of the maximum slip within the cluster. Then

$$MSE = \frac{1}{n} \sum_{i=1}^{n} (s_i - \bar{s})^2 \tag{2.5}$$

with s_i the value of maximum slip in model i, and $\bar{s}$ denotes the average maximum slip within the cluster.

To confirm the uncertainty process, we also calculate the Root Mean Squared Error (RMSE), as shown in Figure 2.5, between the observed values of vertical displacement from the events and the predicted slip values at the same location as the historical data points, or in very close proximity.

$$RMSE = \sqrt{\frac{1}{N}\sum_{j=1}^{N}(\text{historical data} - \text{slip models})} \tag{2.6}$$

With this final step, we obtain the preferred model for each seismic event that contains quantitative data for comparison.

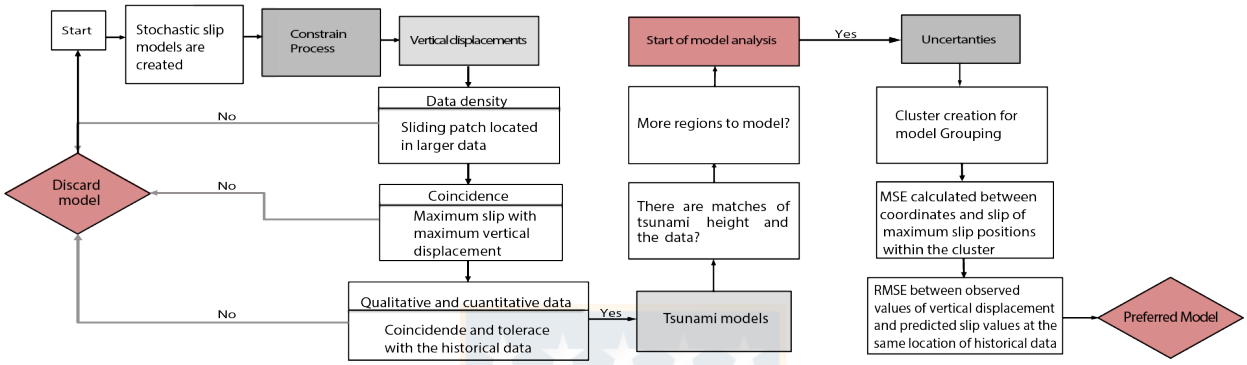

Figure 2.3: Schematic flowchart illustrating the LT approach, constraint processes, and associated uncertainties.

2.4 Results

Through our stochastic modeling approach, we generated thousands of potential rupture scenarios. Figure 2.4 illustrates three key representative models that characterize the rupture patterns of three historical seismic events in central Chile.

For the 1730 earthquake, 18 models met all historical displacement and tsunami constraints. These models comprised 500 subfaults distributed along estimated ruptures between 28°S and 37°S latitude and between 74°W and 70°W longitude, with slip concentrations predominantly located at 33°S and 72°W in the segment closest to the trench (See Figure 2.4,2.7).

For the 1906 event, only six models passed the constraint process, which was notably limited due to the scarce information available regarding slip distribution along its potential rupture. We generated 800 subfaults that were tested across different rupture boundaries and trench segments to better define slip patches and their resolution. This approach considered that the logic tree method has been tested primarily for large events (e.g., Cifuentes-Lobos et al., 2023) rather than smaller events of this type. The estimated rupture occurred between 37°S and 33°S latitude and between 76°W and 70°W longitude, showing a maximum slip patch between 33°S and 34°S (See Figure 2.4,2.8).

Regarding the 1985 event, 44 models satisfied all historical constraints. These models were constructed with 800 subfaults along 32°-35°S latitude and 74°-73°W longitude, showing maximum slip patches at 33.5°S (See Figure 2.4,2.9). The rupture reconstructions for all three events (1730, 1906, and 1985) were generated using the same latitude and longitude scale to allow direct comparison (Figure 2.4).

Our analysis estimated two key measurements: the entire slip distribution and the main patches (defined as areas with slip over 2m). The 1730 event ruptured 982 km in total, extending 501 km

north from Valparaíso to La Serena and 481 km south to Concepción. The 1906 event ruptured a total of 596 km, with its main 200 km patch extending from Valparaíso 77 km north toward Papudo and 123 km south to Cahuil. The 1985 event ruptured 373 km in total, with its main 172 km patch extending from Algarrobo 57 km north near to Quintero and 115 km south to Rio Rapel. See Figures 2.7, 2.8 and 2.9

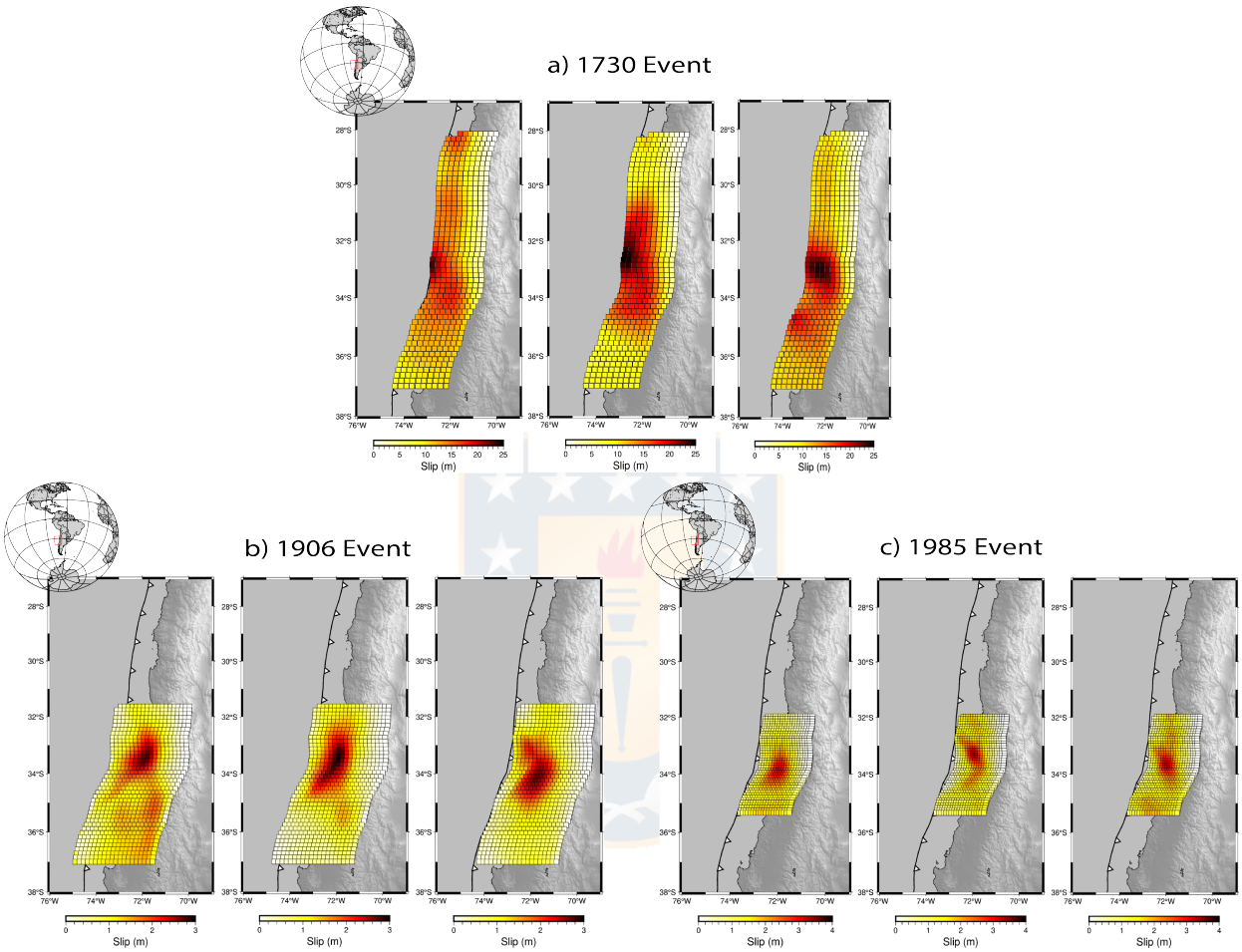

Figure 2.4: First view of restricted rupture models for Historical Earthquakes in central Chile. Panel a) shows the 1730 earthquake, with a clear indication of a shallow rupture. Panel b) the 1906 earthquake and panel c) the 1985 earthquakes display a deeper rupture along the slab in comparison to the 1730 seismic event.

The reconstructed models were subsequently analyzed to assess their associated uncertainties within the constraint process. Statistical analysis was performed by calculating the mean and standard deviation for each model generated for each earthquake, followed by determining the maximum slip location for each constrained model. These results were then clustered to identify trends in terms of slip patch location and magnitude present in Figure 2.5.

For the 1730 event, the primary concentration was identified in cluster 2 (see Figure 2.5 a, b, left column), located in the shallowest part of the slab between 72.8°W longitude and 33°S latitude. Of the 18 models, clustering analysis selected 9 final models, with the mean maximum slip located at 72.1°W and 33.38°S. The clustering process revealed distinct patterns in slip distribution and rupture characteristics among these selected models.

For the 1906 event, the mean maximum slip was positioned at 71.96°W and 33.69°S latitude. Due to the minimal number of highly similar models, clustering analysis proved less significant for this event (see Figure 2.5 a, b, central column). Therefore, statistical analysis was performed individually on each of the six models that passed the initial constraint filtering process.

The 1985 event analysis of 44 models demonstrated a clear trend of maximum slip concentration between 72°-71.7°W and 34°-32.5°S, with mean maximum slip occurring at 71.82° longitude and 33.69° latitude. The cluster analysis identified 29 models with similar characteristics grouped in cluster 1 (see Figure 2.5 a, b, right column), allowing the final error analysis. These models exhibited consistent patterns in their slip distribution and rupture geometry, providing a robust foundation for uncertainty quantification.

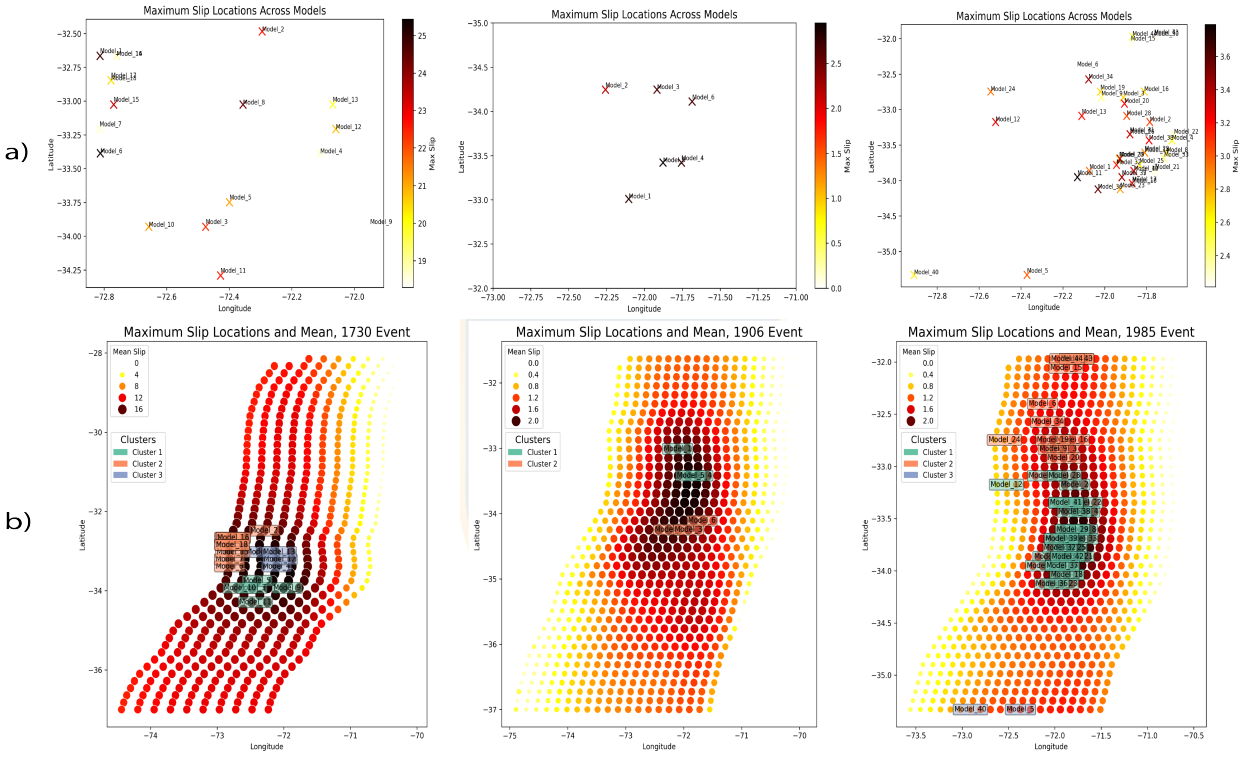

Figure 2.5: Viewing the clustering of models in terms of the maximum slip location for each studied earthquake, compared to the mean slip calculated for all models. Panel a) Initial view shows us where the largest amount of maximum slip is concentrated in terms of longitudes and latitudes, panel b) Clustering location obtained in terms of maximum slip location for 1730, 1906, and 1985 Earthquakes, respectively.

Following cluster identification, we focused our analysis on the clusters containing the highest number of models. For these clusters, we calculated the Mean Square Error (MSE) in terms of both coordinates and slip values between each model and the cluster mean. This approach enabled us to identify preferred models for each seismic event, selected based on minimal error values in both spatial coordinates and slip magnitudes relative to all filtered models within their respective clusters.

To validate our uncertainty analysis methodology, we conducted a characteristic analysis by calculating the Root Mean Square Error (RMSE) between six constrained slip models for the 1906 event, and the quantitative historical vertical displacement measurements (in meters) documented by Carvajal et al. (2019). This analysis aimed to verify if our uncertainty estimation

approach through clustering yielded consistent results with those obtained from quantitative historical validation data. The comparison, visible in Figure 2.6 and Table 2.2, demonstrated satisfactory agreement and showed that the preferred model was ID 5, supporting the reliability of our clustering-based uncertainty assessment method.

Table 2.2: Preferred Models and Their Error Metrics for Historical central Chile Earthquakes

MSE	**1730**	**1906**	**1985**
Model Set 1			
Model ID	17	5	39
MSE coordinates	1.30×10^{-3}	1.01×10^{-2}	1.36×10^{-3}
MSE maximum slip	1.43	1.27×10^{-2}	1.32×10^{-1}
Model Set 2			
Model ID	15	2	26
MSE coordinates	1.36×10^{-2}	2.17×10^{-2}	1.50×10^{-3}
MSE maximum slip	2.07	5.25×10^{-3}	1.02×10^{-1}

Note: MSE = Mean Square Error. Coordinate MSE is calculated in decimal degrees. Maximum slip MSE is calculated in meters.

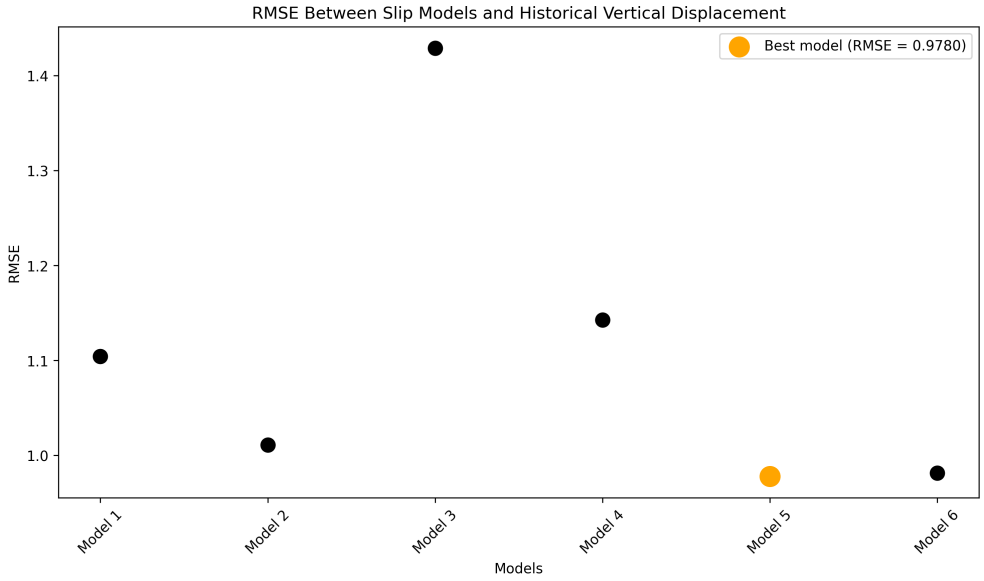

Figure 2.6: RMSE Between Final Slip Models and Historical Vertical Displacement for 1906 seismic event.

2.5 Discussion

Our analysis provides new evidence supporting the contrasting rupture patterns observed in the central Chile subduction zone. The historical seismic record examined in this study reinforces the concept identified by Carvajal et al. (2019) of alternating rupture modes: occasional exceptional tsunamigenic events (exemplified by the 1730 earthquake) interspersed with sequences of moderate-magnitude, deeper earthquakes that produce limited tsunami effects (as seen in the 1822, 1906, 1985, and 2017 events).

The slip distributions reconstructed in our study reveal a persistent spatial segregation of rupture areas through time. This observation, combined with the current state of strain accumulation in the shallow portion of the megathrust, suggests the region may be accumulating potential for a future large-magnitude event with significant tsunami generation capacity. The spatial extent of such an event would likely be constrained by the rupture zones of the 2010 Maule earthquake to the south and the 2015 Illapel earthquake to the north.

2.5.1 Preferred Models

The slip distribution analysis of the 1730 seismic event revealed a shallow large rupture pattern extending along 982 km of the Chilean coast, extending 501 km to the north, and 481 km to the south, present in panel a) of Figure 2.7. The maximum slip of 28 meters was concentrated at 33°S latitude and 72.8°W longitude (Figure 2.7c), with predominant slip occurring within the uppermost 20 km of the subduction interface (2.7b). The event's estimated magnitude was M_w 9.1, with its effects documented from south of Copiapó to north of Concepción. Historical tsunami records recopilated by Carvajal et al. (2017); Stewart (2019); Carvajal et al. (2019) indicate maximum wave heights of approximately 10 meters in Valparaíso, 8 meters in Penco, and far-field effects reaching 2 meters along the Japanese coast.

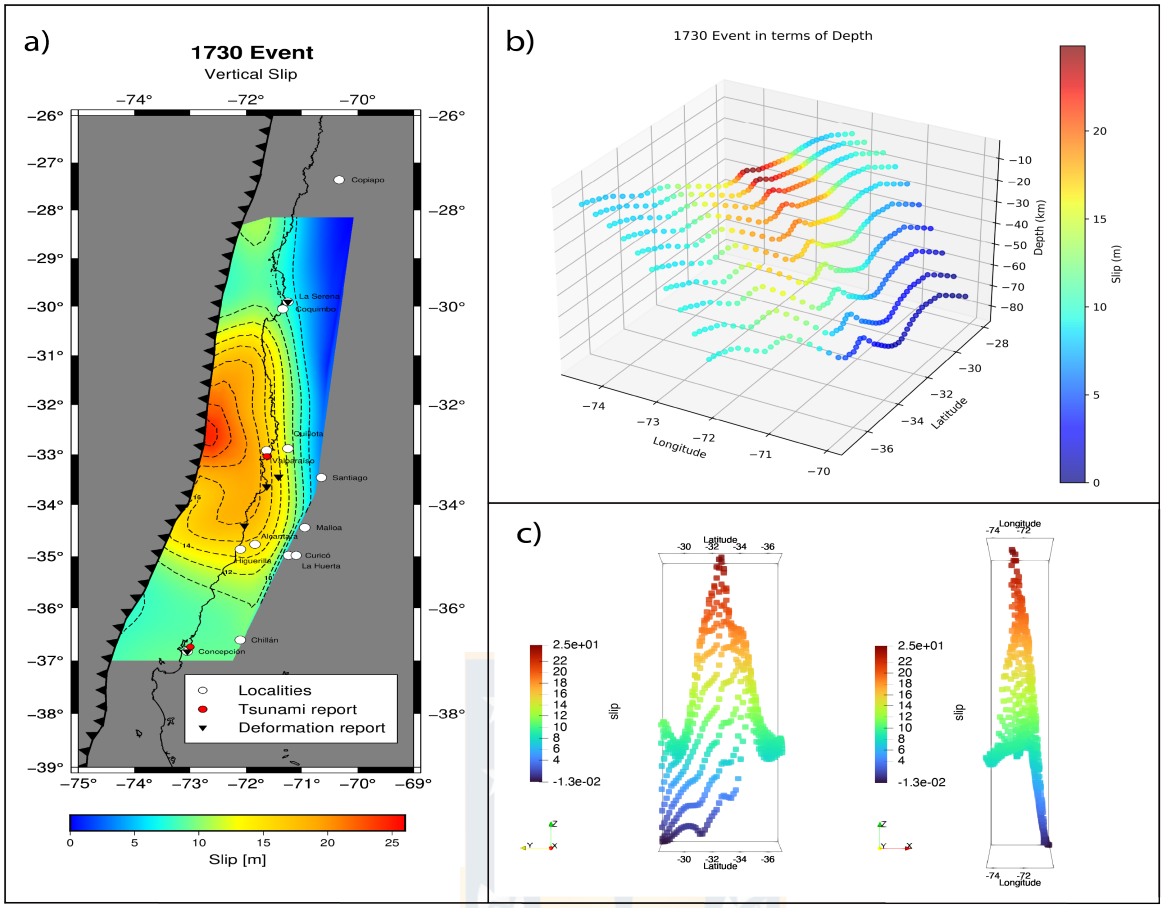

Figure 2.7: Slip distribution characterization of the preferred model for the 1730 central Chile earthquake. (a) Spatial distribution of slip magnitude across the rupture zone, projected onto the subduction interface. (b) Cross-sectional view showing slip distribution with depth, highlighting variations in the dip direction. (c) Maximum slip projections along latitudinal and longitudinal axes indicate primary zones of displacement. The color scale represents slip magnitude in meters.

This configuration better explains the reported tsunami heights and inundation levels in historical records, as explained by Kanamori (2014). The closer the seismogenic zone extends to the trench, the more tsunamigenic potential future earthquakes in this area may have. Similar rupture patterns with maximum slip near the trench have been observed in other major events, such as the Tohoku-Oki earthquake (e.g., Iinuma et al., 2011; Ozawa et al., 2011; Fujiwara et al., 2011; Zhou et al., 2014; Lay, 2018). Some insights from our 1730 rupture model include uplift along the coast of Santo Domingo, Estero Yali, and Laguna Bucalemu near Farellones, where the mechanism differs from the 1751 event that lowered and flooded the ground, while the 1730 event raised and dried it (Stewart (2019)). The uplift is not explained by the 1730 event itself, but rather as a product of the Pichilemu and Santo Domingo segment that separates, acting as a boundary and being modified in each earthquake. While the rupture wasn't as extended to the south, our models were able to reconstruct homogeneously without latitude biases despite having fewer data points in the north.

The 1906 event exhibited a deeper rupture pattern, with slip distribution extending along 596 km of the coastline, but the main patch concentrated in 200 km, extending 77 km north

(to Papudo) and 123 km south (Cahuil) (Figure 2.8a). The maximum slip was 3.2 m, located at approximately 40 km depth within the slab (Figure 2.8b), concentrated near 72°W along the dip direction (Figure 2.8c). The earthquake, with an estimated magnitude of M_w 8.1, primarily affected the coastal region from Illapel to Tomé. This deeper rupture configuration contrasts notably with the shallow rupture pattern observed in the 1730 event. The earthquake caused coastal uplift, strong ground shaking, and a relatively minor tsunami, with severe infrastructural damage reported along nearly 600 km of coastline (Carvajal et al. (2019)). Despite the extensive rupture patch and coastal uplift data, the reported tsunami did not exceed 3 meters in run-up height between Concón (32.9°S) and Puerto Saavedra (38.8°S)

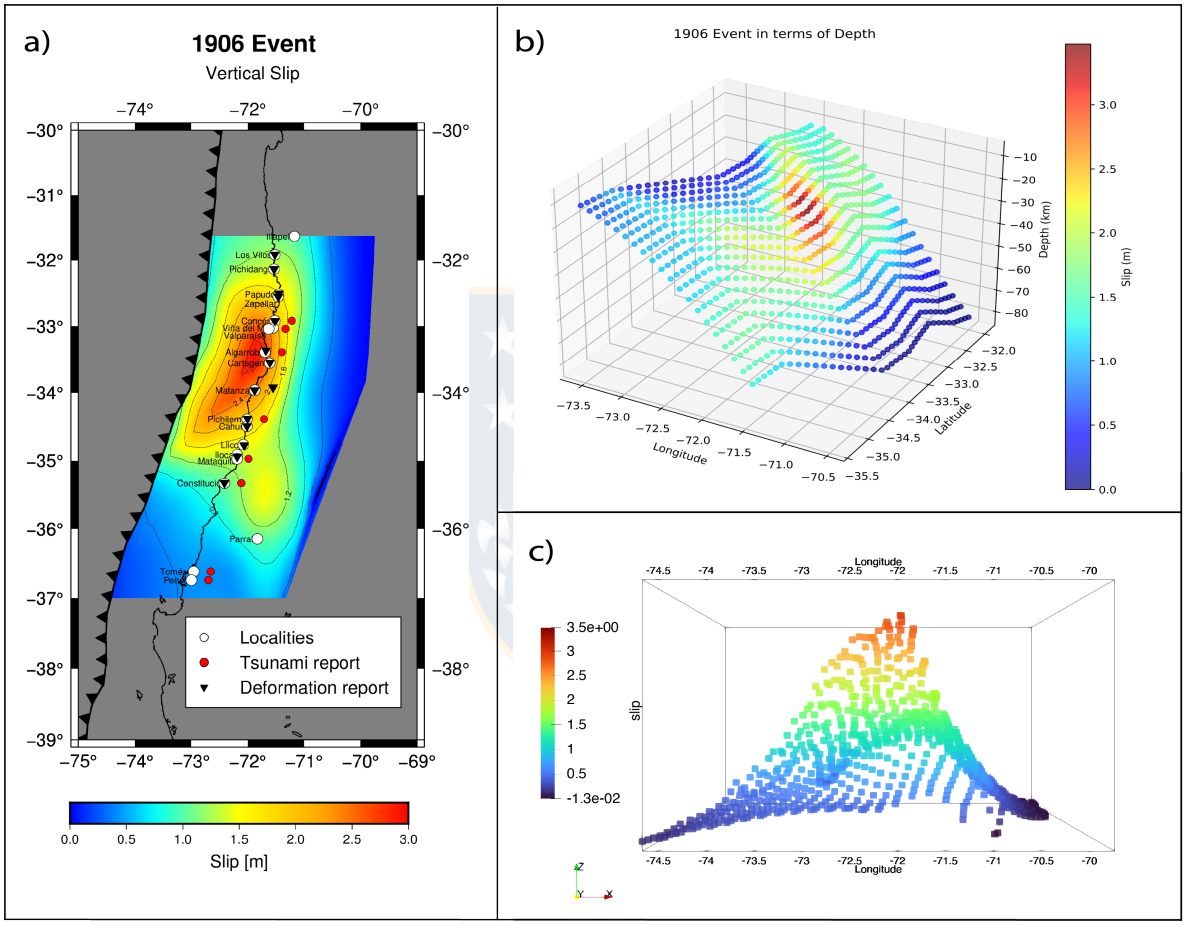

Figure 2.8: Slip distribution characterization of the preferred model for the 1906 central Chile earthquake. (a) Spatial distribution of slip magnitude across the rupture zone, projected onto the subduction interface. (b) Cross-sectional view showing slip distribution with depth, highlighting variations in the dip direction. (c) Maximum slip projections along latitudinal and longitudinal axes indicate primary zones of displacement. The color scale represents slip magnitude in meters.

The 1985 earthquake exhibited the smallest extent of rupture of the three events, spanning a total of 373.61 km along the subduction zone, with the main patch concentrated at 172 km, extending from Algarrobo 57 km north (near Quintero) and 115 km south (Rio Rapel) (Figure 2.9 a). The event, with an estimated magnitude of M_w 8.0, caused documented damage from Los Vilos to Constitución city's (Wood et al. (1987)). The maximum slip was 4 meters concentrated

between 30-40 km depth along the slab (Figure 2.9b), centered at 72°W longitude and 33.5°S latitude (Figure 2.9c). Although predominantly deep, this slip distribution pattern was relatively shallower compared to the 1906 event.

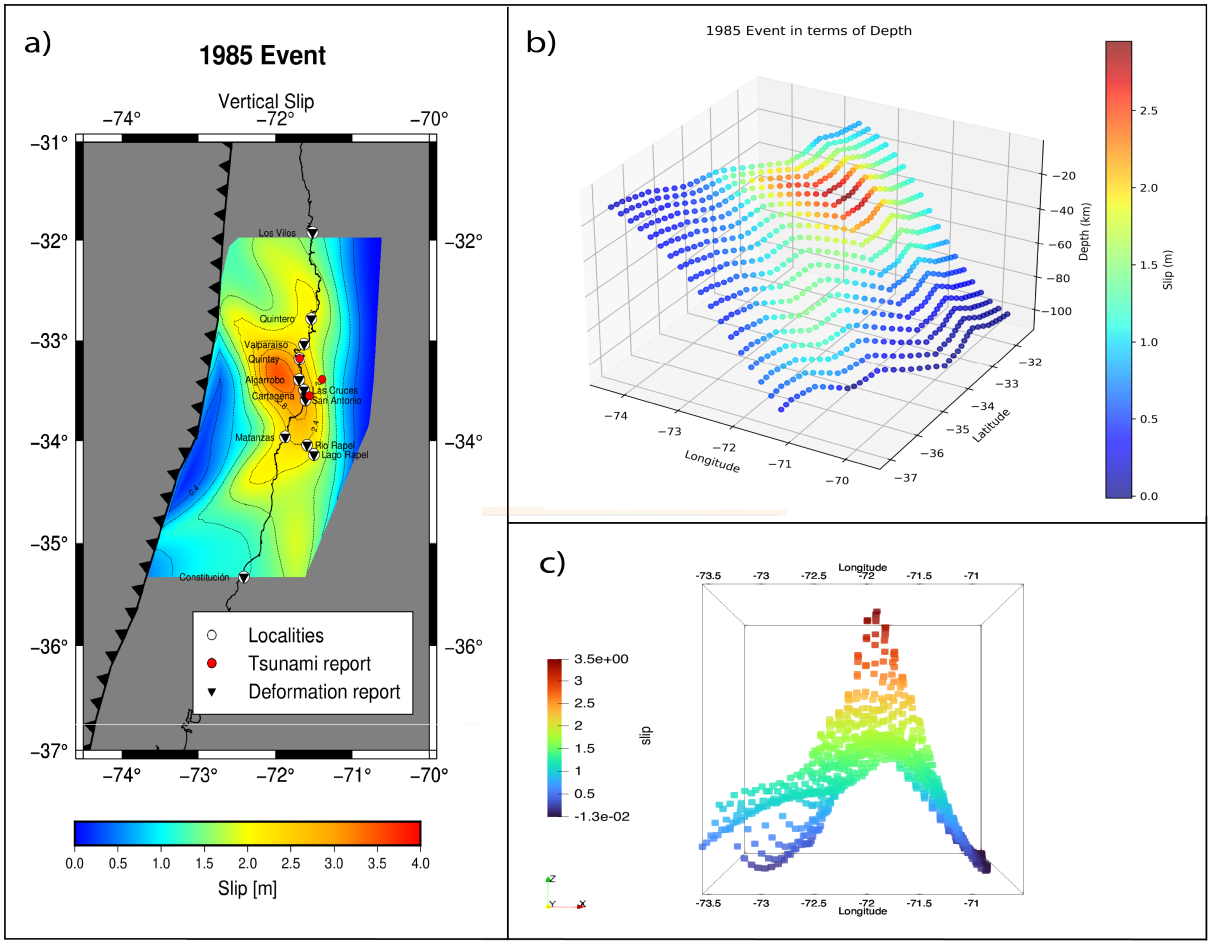

Figure 2.9: Slip distribution characterization of the preferred model for the 1985 central Chile earthquake. (a) Spatial distribution of slip magnitude across the rupture zone, projected onto the subduction interface. (b) Cross-sectional view showing slip distribution with depth, highlighting variations in the dip direction. (c) Maximum slip projections along latitudinal and longitudinal axes indicate primary zones of displacement. The color scale represents slip magnitude in meters.

This is the most recent and best studied of the three events. Although predominantly deep, this slip distribution pattern was relatively shallower compared to the 1906 event, as shown in Figure 2.10. Models such as those by Madariaga (1998), Comte et al. (1986), Bravo et al. (2019) and Carvajal et al. (2019) for the 1985 event show rupture and slip patterns similar to ours, along with predicted coseismic coastal uplift that correlates with our observations.

Taking into account the fault geometry of central Chile, the seismogenic zone spans at least 180 km along the coast in terms of dip, reaching depths of up to 60 km (Moreno et al. (2012); Metois et al. (2016); Carvajal et al. (2017)). Consequently, our modeling reveals two primary rupture modes for this segment: moderate to large earthquakes (Mw 7.8-8.3) typically rupture isolated patches within this segment and predominantly affect deeper portions of the seismogenic interface (close to 40 km from the trench), resulting in limited tsunami generation; while great

earthquakes (Mw $>$ 8.5), such as the 1730 event, can rupture the entire width and length of the seismogenic zone, propagating through shallow segments (within 20 km from the trench) with significantly greater tsunamigenic potential. This dichotomy in rupture patterns explains the contrasting tsunami impacts observed in historical records recollected by Stewart (2019); Carvajal et al. (2019); Comte et al. (1986), with the 1730 earthquake generating waves up to 10 meters high compared to the modest 3-meter run-up heights from the 1906 and 1985 events.

Finally, it's interesting to note the difference between the total slip patch and the main patch (areas with slip $\geq$ 2 m) defined in our work. This definition produces a significantly larger main patch for the 1730 event compared to the relatively smaller main patches for the 1906 and 1985 earthquakes. This distinct pattern in the slip distribution could be valuable for future research in this segment.

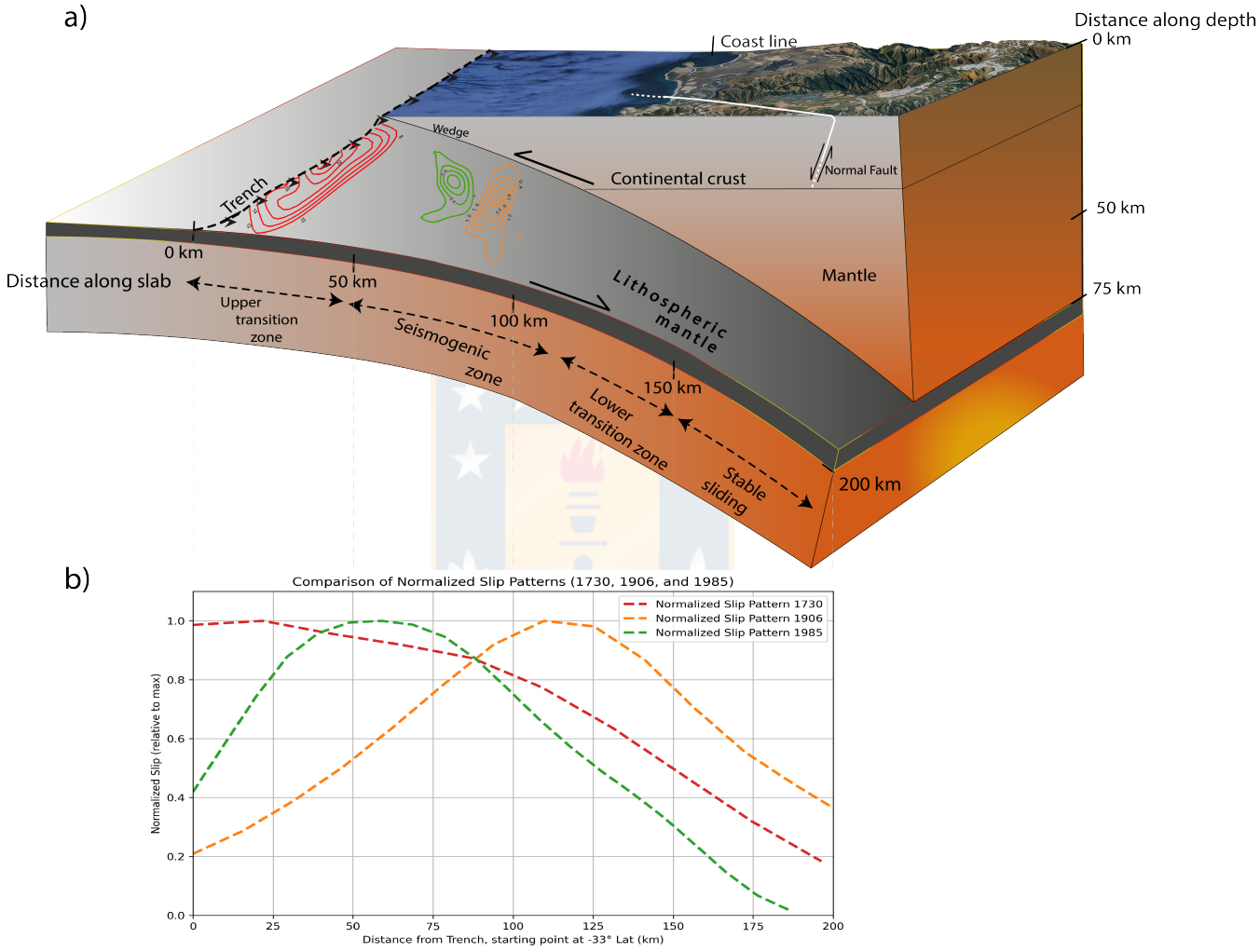

Figure 2.10: Spatial characterization of megathrust rupture domains along the Chilean Subduction Zone. (a) Cross-sectional view showing rupture contours in the Valparaíso region plotted against distance along slab (x-axis) and depth (y-axis). Colored contours represent main rupture patterns from our analysis: the 1730 megathrust event (red), the 1906 earthquake (orange), and the 1985 event (green). The Marga-Marga crustal fault intersection is shown in white. (b) Comparison of normalized slip distributions at 33°S latitude for 1730 (red), 1906 (orange), and 1985 (green) events, demonstrating the systematic variation in rupture depth and extent. Slip values are normalized and plotted against distance along the slab to facilitate direct comparison of rupture characteristics between events.

2.6 Conclusions

In agreement with Carvajal et al. (2017), our findings suggest that the sequential progression from deep ruptures to shallow slip events appears to be a characteristic seismic pattern in this boundary region, where the rupture domains of 1730-type earthquakes converge with those documented in other historical seismic events. This pattern suggests that slip depth along this section of the trench is possibly controlled by the slip history of earthquakes breaking this segment, demonstrating a seismogenic behavior of deep ruptures followed by shallower ones throughout history. The shallowest domain (from trench to 20 km below sea level) can produce large tsunamigenic earthquakes with longer rupture durations than deeper events of similar seismic moments, as seen in the 1730 event. Conversely, the deeper domain (35-55 km depth), characteristic of the 1906 and 1985 events with maximum slip around 40 km depth, tends to generate enhanced short-period energy, affecting both teleseismic and local strong ground motions, as mentioned by Lay et al. (2012) and described by the historical compilation of our events (Roa (2009); Valenzuela Márquez (2012); Urbina-Carrasco et al. (2016); Palacios Roa (2016); Carvajal et al. (2017); Carvajal and Gubler (2017); Stewart (2019); Martínez et al. (2019); Carvajal et al. (2019); Stewart (2020))

Given that the three most recent seismic events primarily involved deeper fault segments, our analysis indicates that significant strain energy may have accumulated in the shallow portions of the subduction interface since the 1730 earthquake, a proposition aligned with observations by Carvajal et al. (2019). This prolonged energy accumulation period of approximately 300 years suggests the potential for significant tsunami generation when released, particularly along the central Chilean coastline as demonstrated by the shallow rupture characteristics revealed in our modeled reconstruction of the 1730 event.

These historical reconstructions provide crucial information to understand the seismic behavior of central Chile and to anticipate future event mechanisms in this segment, as illustrated in Figure 2.10. With an expected seismic event in the Valparaíso gap that could share characteristics with the 1730 earthquake, understanding its slip distribution and rupture mechanism becomes crucial to interpreting the relationship between shallow-large and deep-small earthquakes in this segment. Furthermore, the presence of the Marga-Marga crustal normal fault in Viña del Mar, where our models indicate the largest seismic gap patch (see Figure 2.10), requires special consideration. Historical records document fault-related effects during the 1906 and 1985 earthquakes Thorson (1999); Philippi and Garrido (2016), suggesting potential seismic activity. This scenario bears similarities to the Pichilemu fault system, which experienced triggered crustal seismicity following the 2010 Maule earthquake (Farías et al. (2011)), highlighting the importance of considering crustal fault responses during megathrust events in this region.

The patterns observed in the historical seismic record underscore a fundamental principle in the assessment of seismic hazards: the characteristics of past earthquakes provide crucial constraints on future seismic potential. In the context of the Marga-Marga fault within the Valparaíso seismic gap, this principle suggests treating this structure as potentially active, particularly given its documented responses during the 1906, 1985 and 2010 seismic events.

2.7 Open Research

Example datasets, conferences, and all the code for the stochastic process (LT), constraint process, and uncertainty analyses are available Alvarez-Vargas et al. (2025). For specific code-related questions, please contact the corresponding author.

Chapter 3

Marga-Marga Fault

3.1 Background and Significance

The Marga-Marga fault represents one of the most prominent geological structures in the coastal zone near Viña del Mar, Chile. First documented by Grimme and Álvarez (1964), the fault extends approximately 50 km, with a well-documented 15 km subsegment from Estero Las Palmas to Muelle Vergara that runs beneath the Marga-Marga estuary, bisecting the city(Villavicencio and Suazo (2022); Grimme and Álvarez (1964)). The fault trace is characterized by a subvertical shape towards the mantle, with a strike orientation to the southwest. Regarding movement, although recent studies have predominantly classified it as a normal fault (see Figure 3.3) (e.g., Maldonado et al., 2021; Muñoz et al., 2012; Gana et al., 1996), the limited research on this structure leaves room for alternative interpretations. Thorson (1999) suggests the possibility of strike-slip components in its movement, based on structural evidence and the linear geometry of the fault. This uncertainty in the fault's kinematic behavior underscores the need for more comprehensive structural analysis to fully understand its tectonic role in the region.

3.1.1 Geological Setting and Surface Expression

The surface expression of the fault is particularly evident in the geomorphology of the Marga-Marga valley. Between Viña del Mar and Quilpué, the valley takes the form of a narrow, straight canyon (Figure 3.1, panel b), with a slightly concave map trace towards the northeast. The valley's morphology exhibits a distinct bipartite character: above an altitude of approximately 80 meters, the canyon is relatively wide and intersected by small "quebrada (steep-sided ravine)", while below 200 meters, the gradient of the valley spurs increases dramatically, creating a straight inner canyon with valley wall slopes averaging around 25 degrees (Thorson (1999)).

Field evidence from excavations between Chorrillos and El Salto has revealed significant structural features (Thorson (1999)). The fault zone, exposed in the southwestern valley wall, consists of a brecciated fracture zone in pink granite, ranging in thickness from 0.1-1.2 meters. This zone strikes exactly parallel to the valley and dips 85 degrees to the southwest. The fault architecture includes characteristic features of high-strain deformation: clay-rich, unweathered, greenish-gray fault gouge with en-echelon steps, though notably lacking conspicuous slickenmarks (Figure 3.1, panel c). The gouge material exhibits microscopic particle alignment evidenced by surface sheen, indicating frictional abrasion and shear under high lithostatic stress conditions (Thorson (1999)).

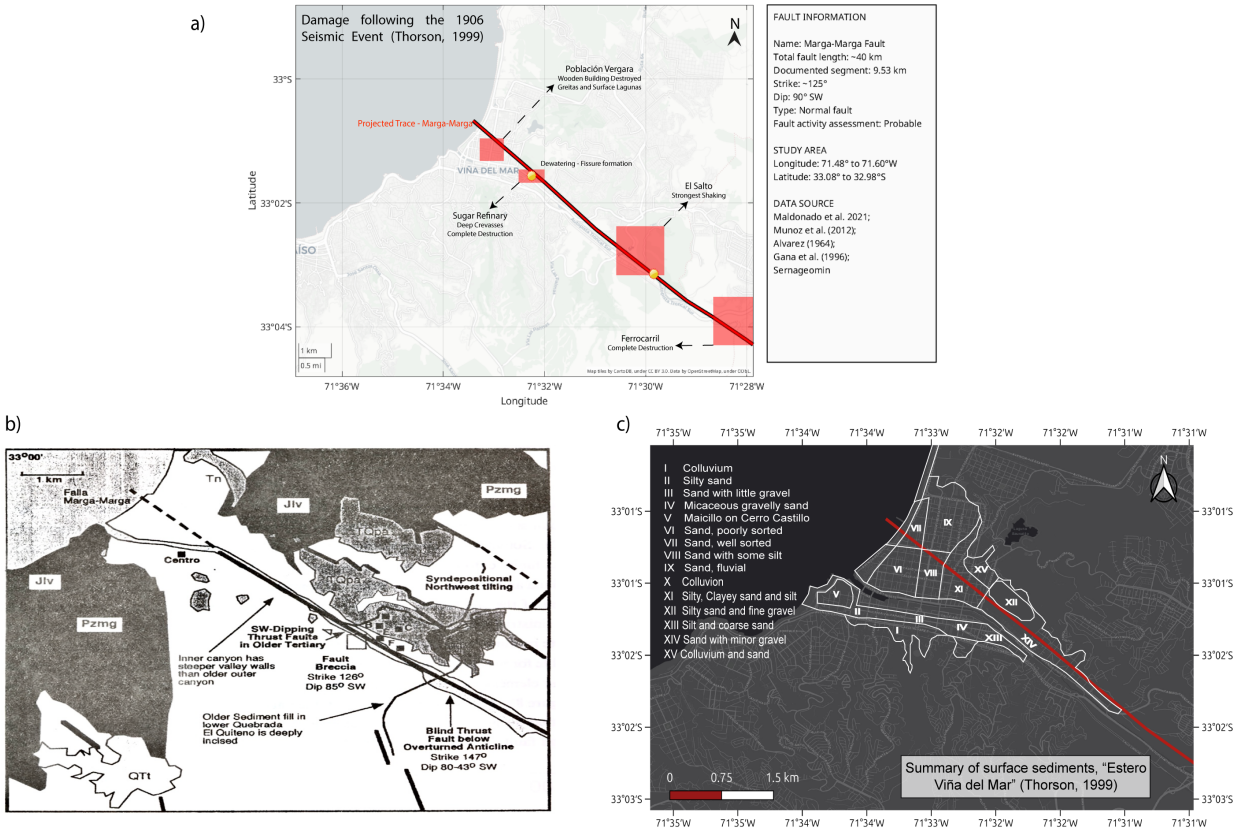

Figure 3.1: Marga Marga setting adapted from Thorson (1999). a) Fault trace, b) Structural features, and c) Surface sediments.

3.1.2 Historical Seismic Response

The spatial relationship between the Marga-Marga fault trace and seismic damage patterns has been observed during two major earthquakes that affected Viña del Mar: the events of 1906 and 1985. However, the causal relationship between the fault and these damage patterns remains a subject of scientific research.

During the 1906 earthquake, significant damage was observed at four locations that coincided with the projected trace of the fault (See figure 3.1, panel a). According to historical accounts documented by Rozas and Cruzat (1906), these included:

- Población Vergara, where both wooden and masonry buildings suffered extensive damage
- The intersection of Limache and Valparaíso streets, where witnesses reported the formation of a deep crevasse with water upwelling
- El Salto, where particularly intense shaking was reported
- The railroad section between El Salto and Quilpué, which suffered complete destruction, showing a distinctive deformation pattern. The tracks were described as having a zigzag pattern by Branner (1915). This phenomenon occurred on generally flat terrain, suggesting that the ground was sheared by a horizontal surface rupture.

Branner (1915) recognized that the poor soil performance in Plan de Viña, which included partial liquefaction, was due to the amplification of seismic waves by subsurface soils: "The effects produced during the earthquake were merely the consequence of seismic wave propagation through loose and unconsolidated alluvial soils." During the 1985 earthquake, a different pattern of damage emerged. Saragoni et al. (1985) and Celebi (1987) demonstrated that, in addition to material amplification in the soils, the sedimentary basin itself altered the incoming seismic signal by amplifying ground accelerations, extending the duration of shaking, and adding a long-period harmonic. Pérez and Aguirre (1988) documented unusual soils in building foundations up to 300 meters from the estuary, noting the presence of saturated, highly organic, and very plastic silty-clay at depths between 3 to 6 meters.

The concentration of damage in tall buildings along Avenida San Martín during the 1985 earthquake led to various interpretations. Pérez and Aguirre (1988) attributed this to the location of an ancient river course, and also considered multiple factors, including the potential influence of the fault, though noting that the correlation mechanism remained unclear: "It is evidently related to multiple contributing factors, including site effects, foundation conditions, structural characteristics, the presence and potential activation of the Marga-Marga fault, topographic effects, and seismic wave directionality, among others".

Furthermore, if the near-surface material indeed originates from depth, then a plausible mechanism for its emplacement would be the upward movement of water along a coseismic fracture Thorson (1999), which is consistent with the work of Rozas and Cruzat (1906). This is interesting because could reveal a normal component on the fault mechanisms.

3.1.3 Potential mechanisms of fault-induced effects, according to Thorson (1999)

1. Wave guide: The rock zone (being a low-velocity zone) may have captured, responded to, and concentrated seismic energy propagating outward and upward from the subduction zone earthquake, potentially amplifying ground motions locally.

2. If we consider the secondary effects associated with soil components such as dehydration and consolidation, perhaps the formation of fissures and "lagoons" within the Vergara settlement could have developed above shear fractures

3. The amplification of seismic shaking may have depended on sediment thickness

4. One possibility is that one or more prehistoric fault ruptures occurred, and that sediments associated with the healed ruptures constituted a zone of weakness reactivated by the 1906 and 1985 events.

3.1.4 Potential indicators of fault activation

If we consider that following the 1906 seismic event, there is an absence of historical accounts of surface rupture, except for the opening of a single deep fissure near the sugar refinery, exactly above the fault, this isolated occurrence suggested by Thorson (1999), could potentially be interpreted as an activation signal.

Building upon this potential activation signal, after the 1985 earthquake Celebi (1987) and Gana et al. (1996) reported topographic amplification and destruction in the Beagle Channel area occurred precisely in its northern section (See figure 3.2). Additionally, considering the work of Carpenter et al. (2011), it was noted that the majority of damaged buildings were concentrated in a triangular area coinciding with the Marga-Marga fault zone and underlying soft soils. However, we must consider that Thorson (1999) also points out that any explanation for the damage patterns after this event must account for the fact that severe damage in 1985 did not strictly follow the fault trace, but was concentrated at the outer coast and near the sedimentary basin's head.

More recently, Hernandez et al. (2023) observed fault scarps northeast of the Marga-Marga stream after the 2010 earthquake, and the most affected buildings were generally well-aligned where sediment thickness and basin depths are greatest, corresponding to the possible fault location.

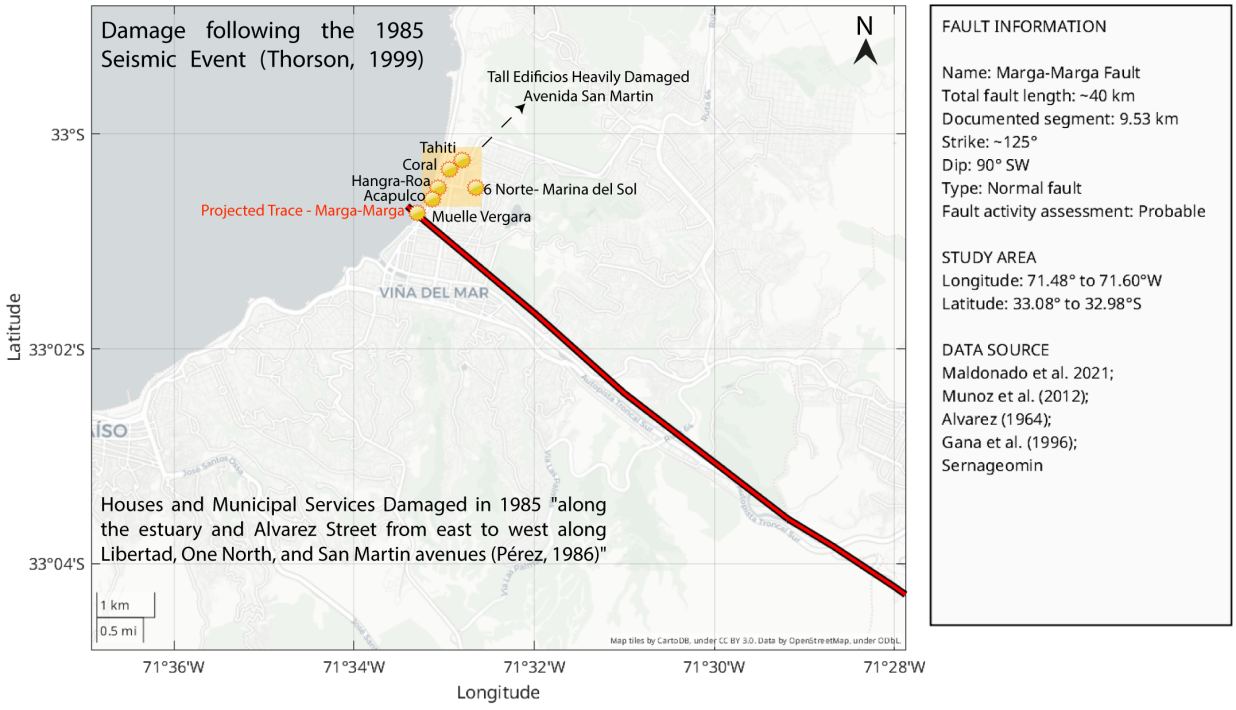

Figure 3.2: Building damage following the 1985 seismic event. Adapted from Thorson (1999).

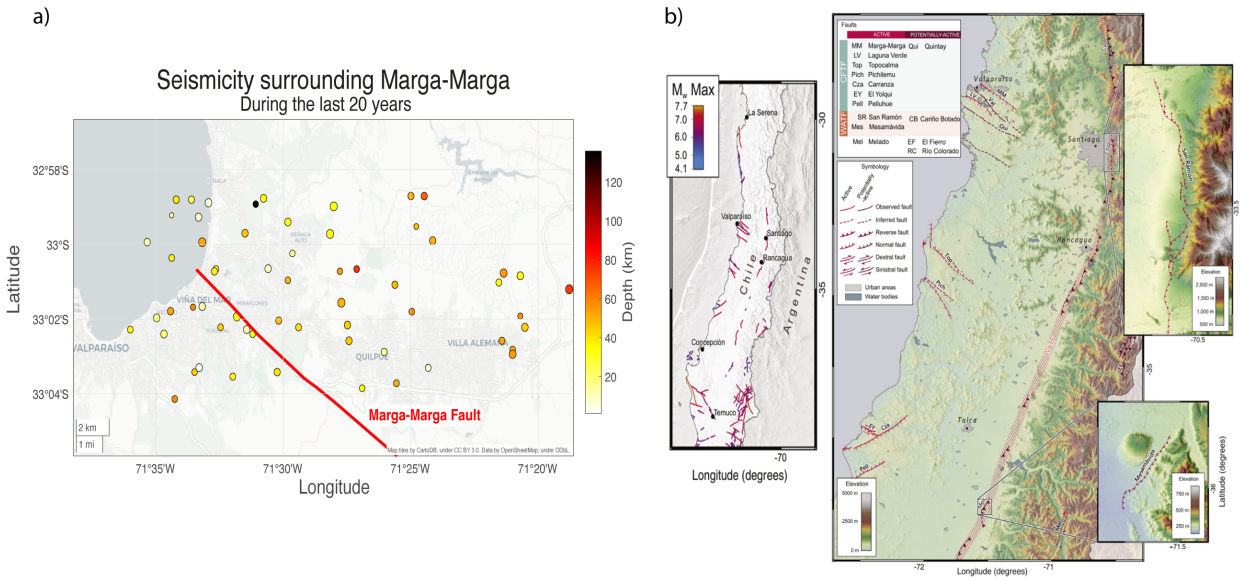

Figure 3.3: Current fault conditions. Panel a) Distribution of seismic events along the fault trace (2000-2024). Panel b) The Marga-Marga structure characterized as a normal fault Maldonado et al. (2021)

It is important to note that while these damage patterns coincide spatially with the fault trace, the mechanisms of interaction between the fault structure and seismic waves remain under investigation. If we noticed the seismicity clusters in Figure 3.3, panel a) surrounding the fault in recent years do not show clear signals of activity related to the fault; however, this could be attributed to insufficient data near the trace to capture relevant signals. Additional seismic data would allow us to not only identify earthquake concentration patterns but also analyze their focal depths, potentially revealing the fault "vertical" structure. Moreover, a larger seismic dataset would enable focal mechanism analysis, offering insights into the stress patterns and kinematics of this fault system. Research on seismicity during the 1985 or 2010 events would be valuable in this context, but the historical data remain limited.

3.2 Coulomb Failure Stress (CFS)

Based on the historical evidence of possible fault interaction and localized damage patterns, a quantitative assessment of stress transfer between the subduction zone and the Marga-Marga fault is warranted. To evaluate this mechanical relationship systematically, we analyze potential triggering mechanisms through stress transfer calculations

We will assess stress changes induced by both the Marga-Marga crustal fault displacement and subduction events occurring within the segment. The analysis employs a two-step approach: first, computing the three-dimensional strain field using elastic half-space displacement calculations, and second, deriving stress changes by applying elastic tensors to the calculated strain field.

The methodology involves resolving both shear and normal stress components across a three-dimensional grid and along predetermined receiver fault planes. These receiver faults are characterized by specific strike, dip, and rake parameters. The resulting shear stress changes will be governed by the geometric and kinematic properties of both the Marga-Marga fault and the subduction fault, as well as the receiver fault geometry, including its rake. In contrast, normal stress changes will be independent of the receiver fault rake.

To evaluate the impact of stress changes on fault stability, we will utilize the Coulomb failure criterion $\Delta\sigma_f = \Delta\tau_s + \mu'\Delta\sigma_{n'}$, presented in Figure 3.4. In this equation, $\Delta\sigma_f$ represents the change in failure stress on the receiver fault caused by slip on the Marga-Marga crustal fault and subduction zone, $\Delta\tau_s$ is the change in shear stress, and $\Delta\sigma_n$ is the change in normal stress. The parameter μ' denotes the effective coefficient of friction on the faults.

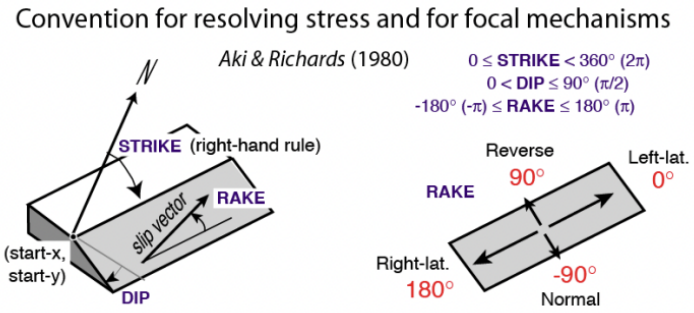

Figure 3.4: Convention for Coulomb stress change on receiver faults by Toda et al. (2011)

This study analyzes potential triggering mechanisms between major subduction events and the Marga-Marga fault through systematic stress transfer calculations. Our analysis focuses on three historical earthquakes (1730, 1906, and 1985) and their associated coseismic slip distributions, on the receiver Marga-Marga fault. The methodology employs AutoCoulomb (Wang et al. (2021)), an iterative implementation of the Coulomb failure model that calculates stress changes in multiple geometric configurations, and previous work in this criteria, such as Cortés-Aranda et al. (2022).

3.2.1 Coulomb Stress Transfer Framework

To properly interpret our results, it is essential to understand the mechanical components that govern fault activation through stress transfer. The Coulomb failure criterion provides a framework for evaluating how stress changes induced by one earthquake can affect the stability of nearby faults.

Components of Stress Transfer

Following the convention used in AutoCoulomb (Wang et al., 2021), the change in Coulomb failure stress ($\Delta\sigma_f$) is expressed as:

$$\Delta\sigma_f = \Delta\tau_s + \mu'(\Delta\sigma_{n'})$$

Where:

Shear Stress ($\Delta\tau$): Represents forces acting parallel to the fault plane in the expected slip direction. Positive shear stress changes promote slip along the fault, while negative changes inhibit slip.

Normal Stress ($\Delta\sigma_n$): Acts perpendicular to the fault plane. Under this convention, positive $\Delta\sigma_n$ represents reduced clamping (unclamping or extension), which decreases the frictional resistance to sliding. Conversely, negative normal stress (increased compression) further clamps the fault, inhibiting failure.

Stress Transfer Thresholds

Based on Freed (2005), an increase in Coulomb stress of 0.1 to 0.3 MPa (1 to 3 bars) is generally sufficient to trigger seismicity, whereas reductions of the same amount can effectively suppress them. This threshold emerges from empirical observations across numerous aftershock studies, rather than being determined by specific fault properties or rock mechanics parameters. It is worth noting that while this threshold value serves as a useful generalization, actual fault response depends on multiple factors including pre-existing stress conditions and seismic cycle stage. This threshold provides a critical benchmark for evaluating the potential triggering effects observed in our analysis.

3.2.2 Fault Parameters for Coulomb Stress Analysis

For the Coulomb stress transfer calculations, we adopted the geometric and kinematic parameters of the Marga-Marga fault based on the comprehensive fault database compiled by Maldonado et al. (2021). These parameters represent the most up-to-date characterization of active and potentially-active continental faults in Chile. Table 3.1 summarizes the fault parameters used in our analysis.

Table 3.1: Geometric and kinematic parameters of the Marga-Marga fault used for Coulomb stress calculations.

Parameter	Value	Description
Strike	125°	Orientation of the fault trace measured clockwise from north
Dip	90°	Vertical inclination of the fault plane
Rake	-90°	Slip vector indicating pure normal faulting
Depth	10 km	Considering the shallow part of the fault
μ'	0.3	Effective coefficient of friction height

The parameter of μ was selected based on González et al. (2020) and Cortés-Aranda et al. (2022), and the fault parameters are consistent with the structural evidence presented by Maldonado et al. (2021), who characterized the Marga-Marga structure as a normal fault based on field observations and geomorphological analysis. The pure normal mechanism (rake = -90°) indicates vertical motion with the hanging wall moving downward relative to the footwall.

3.3 Results of Coulomb Stress Analysis

Our Coulomb stress transfer analysis between historical earthquakes and the Marga-Marga fault reveals significant stress loading patterns. This research was conducted in collaboration with Dr. Juan Gonzalez, whose valuable contributions to data collection and processing enhanced our Coulomb stress modeling as part of ongoing collaborative research on the Marga-Marga fault. While all three analyzed seismic events (1730, 1906, and 1985) induced positive Coulomb stress changes on the receiver fault, we observed substantial variations in both magnitude and spatial distribution of stress across these events.

3.3.1 Regional Coulomb Stress Patterns

The regional Coulomb stress transfer analysis reveals distinct patterns for each of the three historical earthquakes studied (Figure 3.5). These patterns provide insight into how subduction events

affect the broader tectonic setting within which the Marga-Marga fault is situated.

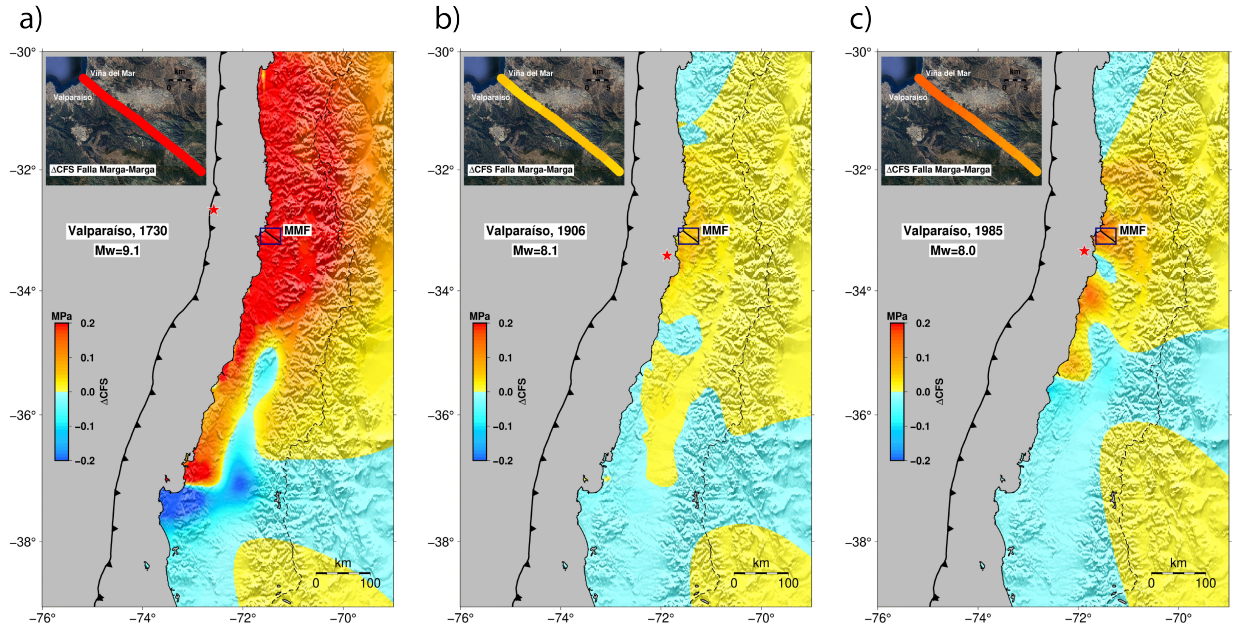

Figure 3.5: Regional Coulomb stress changes induced by the (a) 1730 (Mw 9.1), (b) 1906 (Mw 8.1), and (c) 1985 (Mw 8.0) earthquakes. The Marga-Marga fault (MMF) is indicated by the blue rectangle. Red star indicates the maximum slip location. Color scale shows stress changes in MPa. The color scale for all regional stress maps has been standardized to a range of -0.2 to 0.2 MPa to facilitate direct comparison between the three seismic events.

The 1730 event (Mw 9.1) generated an extensive area of positive stress change (yellow to red colors) throughout the coastal region of central Chile (Figure 3.5a). The Marga-Marga fault is situated entirely within this high-stress zone, experiencing uniformly positive Coulomb stress changes. The regional pattern shows stress values exceeding 0.1 MPa (1 bar) across much of the study area, with localized areas over to 0.2 MPa (2 bar), intense red colors in colorbar.

In contrast, the 1906 earthquake (Mw 8.1) produced a more homogenous stress pattern (Figure 3.5b). The region surrounding the Marga-Marga fault shows moderate positive stress changes, predominantly in the range of 0 - 0.05 MPa (0 - 0.5 bar), predominantly in the yellow to orange range in colorbar. While these values represent positive stress changes, they remain below the commonly accepted triggering threshold of 0.1 MPa (1 bar) as established by Freed (2005). The stress field exhibits a complex spatial distribution with areas of stress shadow (negative stress changes) developing south of the fault zone, while the fault itself remains within a positive but sub-threshold stress lobe.

The 1985 event (Mw 8.0) created a north-south elongated stress pattern with positive values concentrated along the coastal areas (Figure 3.5c). The Marga-Marga fault intersects this positive stress zone, with values ranging from approximately 0.05 to 0.15 MPa (0.5-1.5 bar), orange to red colors in colorbar. The most significant area of increased stress can be observed in the upper left portion of map c), near where the Marga-Marga fault begins (33°S, 72°W), with other nodule close the 34°S.

The Marga-Marga fault consistently falls within zones of positive stress change for all events, suggesting a persistent mechanical coupling between subduction earthquakes and this crustal structure. It is noteworthy that despite the 1985 event being of lower magnitude than the 1906 earth-

quake, it appears to have more effectively triggered activity along the Marga-Marga fault. This observation suggests that earthquake magnitude alone is insufficient to predict crustal fault response, and that other factors such as rupture characteristics, stress transfer directionality, or pre-existing fault conditions may play determinant roles in the activation process.

Regarding the maximum displacement location of these events, red star in panel a) of Figure 3.5, the 1730 case presents an interesting observation. The star marks the area of greatest slip in our source model, which was used as input for our Coulomb stress calculations. Notably, this location coincides with a region showing high positive Coulomb stress values in our analysis. This particular event (See Figure 2.7) may share characteristics with the Tohoku-oki 2011 earthquake (see e.g. Iinuma et al. (2011), Ozawa et al. (2011), Fujiwara et al. (2011)), where significant crustal displacement occurred near the trench. Through our reconstruction of the 1730 event, we have been able to identify this maximum displacement zone, but this does not necessarily represent the beginning of the nucleation of the earthquake. In terms of latitude, however, our estimated position correlates well with the historical location documented at approximately 32.5°S NOAA National Centers for Environmental Information (n.d.), representing an important validation point for our modeling approach.

3.3.2 Correlation Between Regional and Fault-Specific Stress Patterns

The fault-specific analysis of Coulomb stress changes along the Marga-Marga fault shows consistency with the regional stress patterns described above. For each earthquake, the stress values measured directly on the fault reflect the broader regional distribution while providing more detailed insight into the mechanical loading experienced by this structure, in terms of shear, normal and coulomb stress.

We analyzed the stresses along the Marga-Marga Fault, identifying the maximum and minimum values in order to compare where the maximum stress occurred for each earthquake in terms of longitude. Unlike Figure 3.5, which used a range of -0.2 to 0.2 MPa to facilitate direct comparison, in this section we present the full stress values measured along the fault to provide a complete picture of the stress magnitudes experienced by the Marga-Marga Fault.

1730 Case

a) Coulomb Stress along the fault:

- Maximum value: 4.6417 bar (0.46417 MPa, around -71.45° longitude).
- Minimum value: 3.1109 bar (0.31109 MPa, near -71.25° longitude).
- The distribution shows an arched pattern with a clear peak in the central region of the fault.
- All values are positive, indicating a generalized increase in Coulomb stress.

b) Shear Stress:

- Maximum value: -0.5440 bar (-0.05440 MPa, around -71.45° longitude).
- Minimum value: -1.6405 bar (-0.16405 MPa, near -71.25° longitude).

- Negative shear values indicate stress forces acting against the fault's natural slip direction, potentially stabilizing the fault segment, whereas positive values would promote movement along the expected slip direction.
- The pattern shows less negative stress (closer to zero) in the central part of the trace.

c) Normal Stress:

- Maximum value: 17.8425 bar (1.78425 MPa, near -71.55° longitude).
- Minimum value: 14.8903 bar (1.48903 MPa, near -71.25° longitude).
- All values are positive and relatively high.
- The distribution shows a descending trend from west to east.

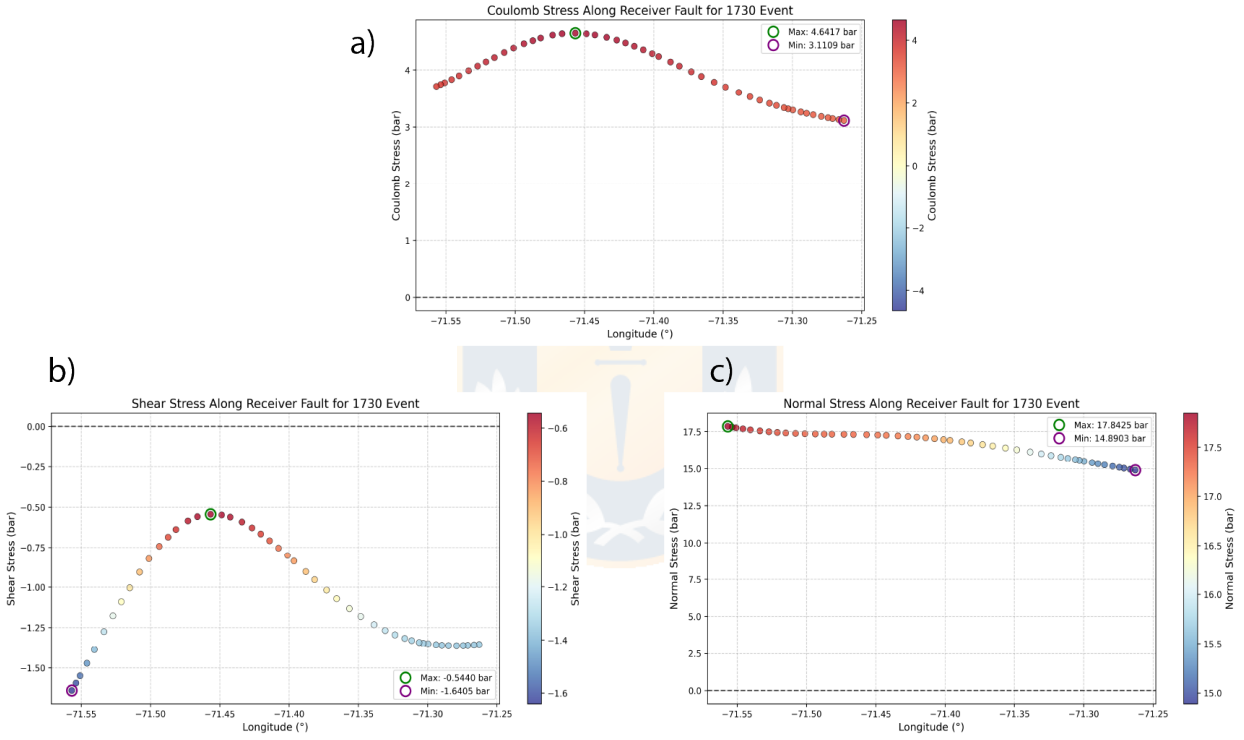

Figure 3.6: Stress distribution along the receiver fault for the 1730 event. a) Coulomb stress, b) Shear stress and c) Normal stress pattern. All panels display stress values (in bars) as a function of longitude (°W) along the fault.

1906 Case

a) Coulomb Stress:

- Maximum value: 0.5852 bar (0.05852 MPa, around -71.40° longitude)
- Minimum value: 0.4242 bar (0.04242 MPa, near -71.50° longitude)
- The distribution shows a wave-like pattern with the highest peak at -71.40° and a notable low point at -71.50°

- All values are positive but significantly lower than those for the 1730 event, indicating a moderate increase in Coulomb stress

b) Shear Stress:

- Maximum value: 0.2477 bar (0.02477 MPa, near -71.55° longitude)
- Minimum value: 0.1207 bar (0.1207 bar = 0.01207 MPa, around -71.50° longitude)
- Unlike the 1730 event, all values are positive, indicating shear in the same direction as the expected slip on the fault
- The pattern shows higher values at the western edge and a dip around -71.50°, followed by moderate values in the central and eastern portions.

c) Normal Stress:

- Maximum value: 1.1841 bar (0.11841 MPa, around -71.40° longitude)
- Minimum value: 1.0078 bar (1.0078 bar = 0.10078 MPa, near -71.55° longitude)
- All values are positive but much lower than for the 1730 event
- The distribution shows an increasing trend from west to east, with a plateau in the eastern segment.

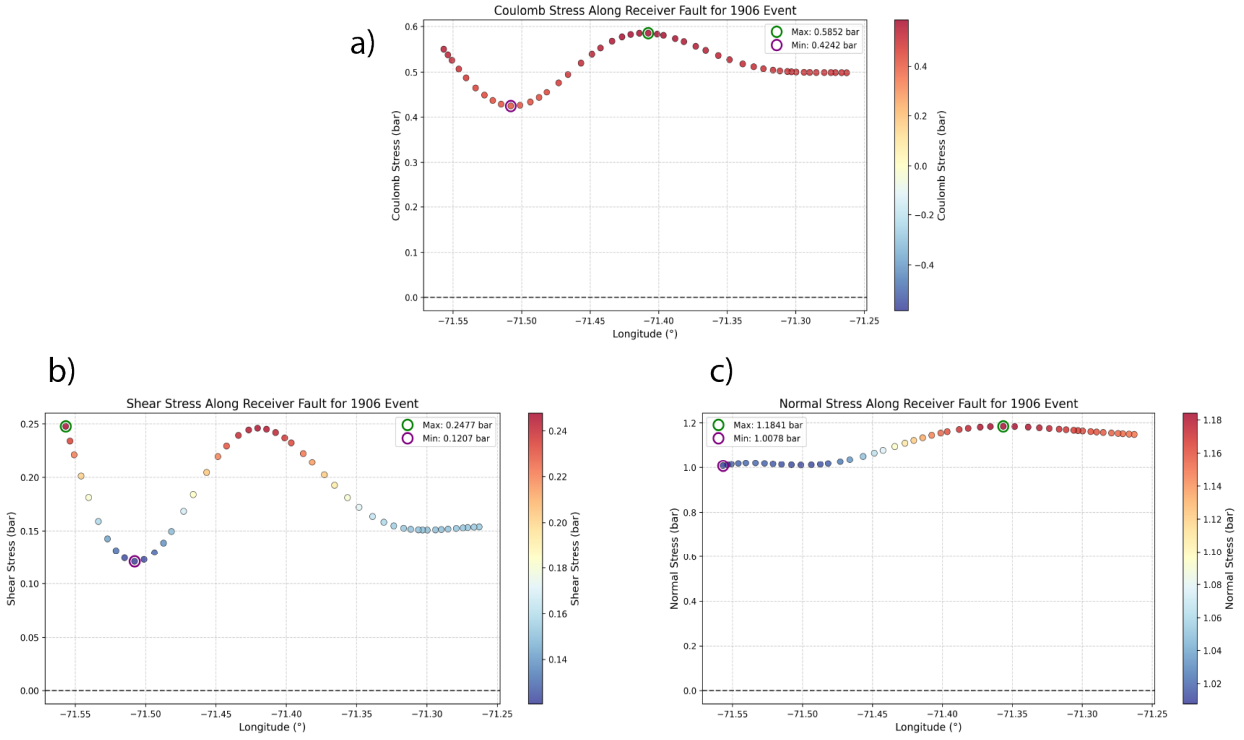

Figure 3.7: Stress distribution along the receiver fault for the 1906 event. a) Coulomb stress, b) Shear stress and c) Normal stress pattern. All panels display stress values (in bars) as a function of longitude (°W) along the fault.

1985 Case

a) Coulomb Stress:

- Maximum value: 1.5692 bar (0.15692 MPa, around -71.53° longitude).
- Minimum value: 0.8706 bar (0.08706 MPa, near -71.25° longitude).
- The distribution shows a consistently decreasing pattern from west to east.
- All values are positive, indicating a generalized increase in Coulomb stress across the fault.

b) Shear Stress:

- Maximum value: 0.6222 bar (0.06222 MPa, near -71.53° longitude).
- Minimum value: 0.2375 bar (0.02375 MPa, near -71.25° longitude).
- All values are positive, indicating shear in the same direction as the expected slip on the fault.
- The distribution follows a similar west-to-east decreasing trend as the Coulomb stress.

c) Normal Stress:

- Maximum value: 3.1830 bar (0.31830 MPa, near -71.55° longitude).
- Minimum value: 2.1106 bar (0.21106 MPa, near -71.25° longitude).
- All values are positive and moderate compared to the 1730 event but higher than the 1906 event.
- The distribution shows a clear decreasing trend from west to east.

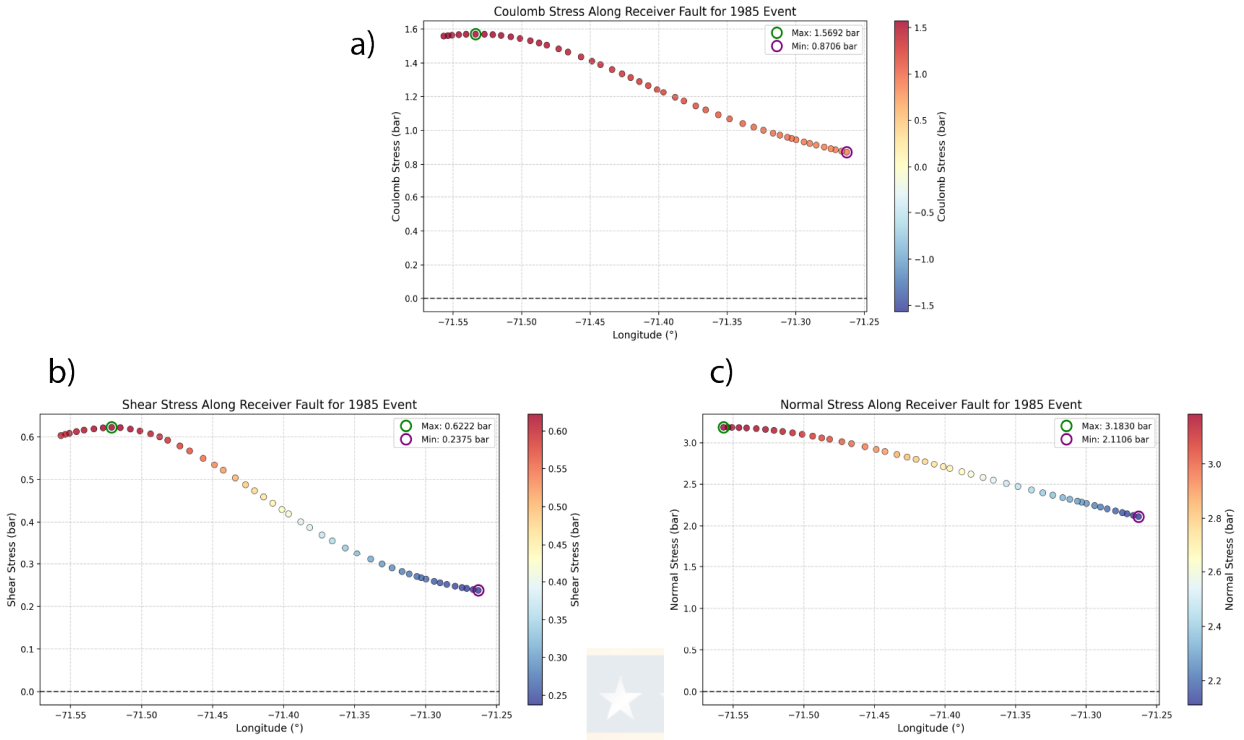

Figure 3.8: Stress distribution along the receiver fault for the 1985 event. a) Coulomb stress, b) Shear stress and c) Normal stress pattern. All panels display stress values (in bars) as a function of longitude (°W) along the fault.

Peak values reached approximately 0.46 Mpa for the 1730 event, 0.06 Mpa for the 1906 event, and 0.16 Mpa bars for the 1985 event. As shown in Figure 3.9, the dominant mechanism in all cases is favorable normal stress (100%), indicating that normal stress changes rather than shear stress primarily contributed to the observed Coulomb stress increases. This spatial and temporal consistency across different subduction events suggests that the Marga-Marga fault has been repeatedly loaded with significant stress changes, potentially explaining its seismic activity following major subduction earthquakes in this region.

A detailed examination of the three cases reveals that the most significant observation from both regional and fault-specific analyses is that two of the three historical earthquakes (1730 and 1985) generated Coulomb stress changes well above the commonly accepted triggering threshold (0.1 to 0.3 MPa or 1 to 3 bars; Freed (2005)) along the entire length of the Marga-Marga fault, while the 1906 event produced positive but sub-threshold stress changes (maximum 0.59 bars) (see Figure 3.9).

Examining the spatial distribution patterns, we observe that the 1730 and 1985 events appear to activate areas near the coast and northern section of the fault with relatively consistent stress gradients. In contrast, the 1906 event exhibits a distinctive non-linear pattern with an undulatory stress distribution. This latter event concentrates stress near the coast, which then dissipates before showing increased stress again in the easternmost section near longitude -71°42. This wave-like pattern might reflect the complex interaction between propagating stress waves from the subduction source and the specific geometry of the Marga-Marga fault, suggesting that stress transfer mechanics depend on rupture characteristics beyond magnitude alone.

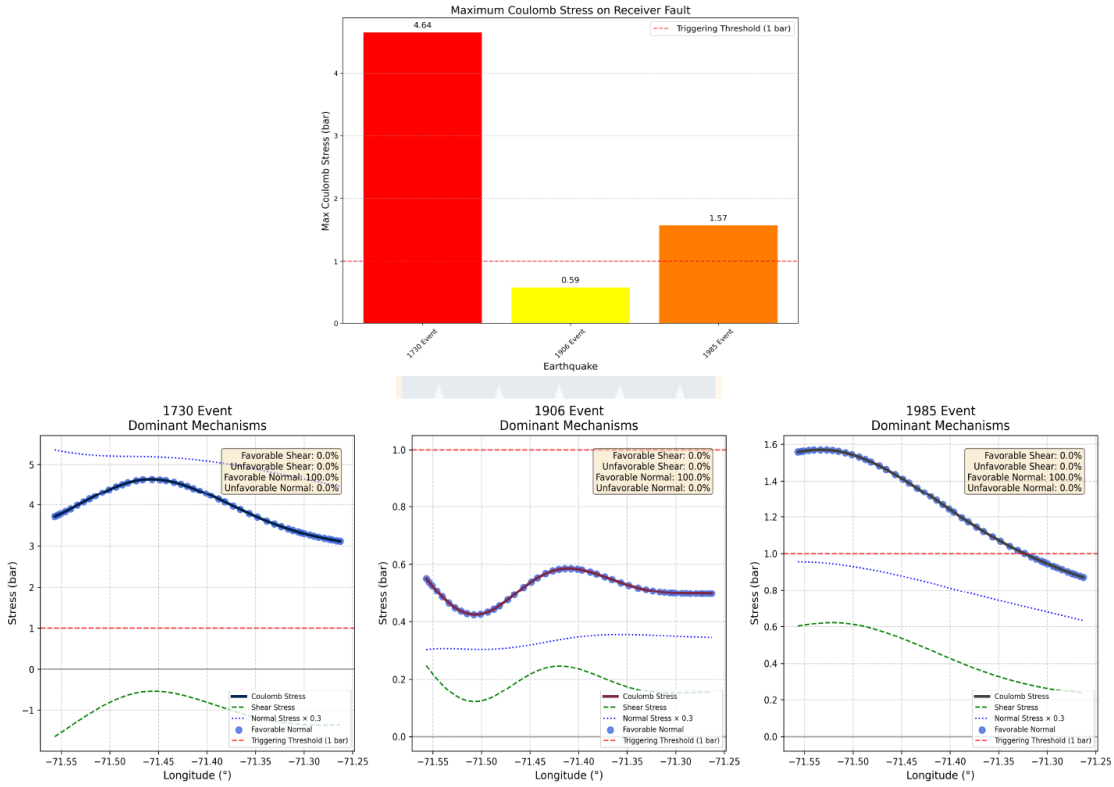

Figure 3.9: Coulomb stress comparison for the Marga-Marga fault from three major historical subduction earthquakes (1730, 1906, and 1985). Top: Bar chart showing maximum Coulomb stress values relative to the 1 bar triggering threshold (red dashed line), highlighting that the 1730 (4.64 bars) and 1985 (1.57 bars) events exceeded this threshold, while the 1906 event (0.59 bars) remained below it. Bottom: Longitudinal stress distribution profiles along the fault. The thick black line represents total Coulomb stress, green dashed lines show shear stress components, and blue dotted lines indicate normal stress (scaled by coefficient of friction 0.3). The red dashed horizontal line marks the 1 bar triggering threshold. Inset boxes display the percentage breakdown of stress mechanisms, revealing 100% favorable normal stress contribution for all events despite varying magnitudes and shear stress directions. Note the different vertical scales, with maximum values of approximately 5 bars (1730), 0.6 bars (1906), and 1.6 bars (1985).

Chapter 4

General Discussions and Conclusions

It is particularly relevant to analyze the relationship between slip distribution patterns and stress concentration on the Marga-Marga fault. The detailed slip reconstructions of historical earthquakes (1730, 1906, 1985) provide the foundation for evaluating their stress transfer potential to crustal faults like Marga-Marga, as rupture characteristics directly influence Coulomb stress distribution patterns. In this context, a detailed comparison of rupture characteristics across the three historical events reveals significantly different stress transfer mechanisms in each case.

These variations in stress transfer efficiency highlight the importance of rupture geometry in controlling upper plate deformation, as different phases of the earthquake cycle, from interseismic loading to coseismic rupture, can produce distinct stress patterns on crustal faults (Loveless et al. (2010)). The paradox that the 1985 event (Mw 8.0) generated greater activation of the Marga-Marga fault than the 1906 event (Mw 8.1), despite its lower magnitude, can be explained by analyzing the specific geometry of the ruptures. The 1985 earthquake presented a slip distribution with maximum values concentrated between 30-40 km depth, centered approximately at 72°W longitude and 33.5°S latitude. This configuration created a spatially concentrated positive stress lobe favorably oriented for the activation of the Marga-Marga fault.

In contrast, the 1906 event, although slightly larger in magnitude, distributed its slip more homogeneously with maximum values shifted southward relative to the fault location. As observed in Figures 3.5 panel b) and Figure 3.7, the stress pattern generated showed positive values but significantly lower (approximately 0.6 bars compared to 1.6 bars from the 1985 event), and with a spatial distribution less optimal for stress transfer to the fault.

The 1730 event, meanwhile, generated the highest Coulomb stress values (approximately 5 bars), with an extensive and shallow rupture that completely covered the area where the fault is located. However, its predominantly shallow rupture depth (within the first 20 km from the trench) contrasts with the intermediate depth of the 1985 event, which possibly created more favorable conditions for concentrating stress specifically on the Marga-Marga fault structure.

These results suggest that the efficiency of stress transfer to crustal structures like the Marga-Marga fault depends not only on the magnitude of the subduction event, but fundamentally on the location, depth, and spatial distribution of slip. Specifically, the 1985 event may have generated a more effective stress field for fault activation due to three main factors:

1. The rupture directivity, which concentrated stress transfer toward the northern zone where the fault is located

2. The intermediate depth of the rupture plane (30-40 km), which fostered more efficient mechanical interaction with the crustal structure

3. The orientation of slip vectors, which was particularly favorable for generating positive normal stress along the orientation of the Marga-Marga fault.

   This relationship between rupture geometry and activation of crustal faults could represent important implications for seismic characterization of this segment, where the combination of subduction earthquakes with varied rupture patterns can generate complex mechanical interactions with surface structures across different temporal scales.

4.1 Discussion of Coulomb Stress Transfer and Historical Seismicity

Building on the observed relationships between slip distribution and stress transfer described above, in the following sections, we examine these patterns in detail, exploring their consistency with historical observations and their implications for understanding the seismic behavior of this crustal structure.

4.1.1 Consistency of Stress Patterns and Historical Damage

The most striking finding from our Coulomb stress analysis is that two of the three historical earthquakes (1730 and 1985) generated positive stress changes exceeding the commonly accepted triggering threshold of 0.1 to 0.3 MPa (1 to 3 bars; Freed, 2005) along the entire length of the Marga-Marga fault, while the 1906 event produced positive but sub-threshold values. Despite these differences in stress magnitudes, all three events showed spatial correlation with historical damage reports documented by Thorson (1999). This observation indicates that the spatial correlation between CFS patterns and fault damage zones observed after 1906 and 1985 events suggests that stress concentrations along the fault trace may influence the location and extent of surface ruptures.

The 1906 earthquake damage patterns, as detailed by Rozas and Cruzat (1906), show notable spatial correspondence with our calculated stress distribution. Four locations along the projected fault trace experienced significant damage: Población Vergara, the intersection of Limache and Valparaíso streets (where a deep crevasse with water upwelling was reported), El Salto (intense shaking), and the railroad section between El Salto and Quilpué. Our analysis indicates that the 1906 event produced Coulomb stress changes of 0.4-0.6 bars along the fault occurring around -71.40° longitude. While these values remain below the 1 bar triggering threshold, the spatial correlation between stress peaks and documented damage suggests that these stress changes may have been one of multiple contributing factors in the complex damage pattern.

Similarly, our analysis of the 1985 earthquake shows stress changes of 0.8-1.6 bars along the fault, with highest values in the western section. This corresponds well with Pérez and Aguirre (1988) documentation of damage concentration in tall buildings along Avenida San Martín and the observations by Celebi (1987)) of topographic amplification and destruction in the Beagle Channel area at the northern section of the fault.

4.1.2 Normal Fault Mechanics and Stress Transfer

A clear finding of our analysis is the dominance of normal stress mechanisms (100%) for all three events. Although we adopted the normal fault classification from previous studies (Maldonado et al. (2021); Muñoz et al. (2012); Gana et al. (1996)) as model input, the resulting stress calculations are compatible with this kinematic assumption and provide a mechanical explanation for the fault

response to subduction earthquakes. It is important to note that the potential for fault reactivation depends on the relationship between fault orientation and the local stress, which can promote different kinematic behaviors. However, in this case, the normal mechanism is most consistent with the Marga-Marga fault's geometry and the stress transfer patterns observed in our analysis.

Our analysis reveals an interesting mechanical behavior regarding stress transfer: despite showing negative shear stress values, the 1730 event produced the highest Coulomb stress changes (4.64 bars) due to overwhelming favorable normal stress contributions. This observation demonstrates that even when shear components work against the direction of slipping of the fault, the unclamping effect of normal stress reduction can completely dominate the trigger mechanism. This balance of competing forces represents a critical consideration when evaluating fault activation potential, as the net Coulomb stress may exceed triggering thresholds even in the presence of unfavorable shear conditions.

In contrast to the 1730 event, our analysis of the 1906 earthquake presents a different scenario. Despite having favorable shear stress (positive values), the 1906 event generated much lower normal stress changes, resulting in a maximum Coulomb stress of only 0.59 bars. This falls below the commonly accepted triggering threshold of 1 bar Freed (2005), highlighting how the magnitude of stress components matters as much as their direction. This finding is particularly significant when interpreting Thorson (1999) observation that the 1906 earthquake resulted in "the opening of a single deep fissure near the sugar refinery, exactly above the fault". While this feature might initially appear to suggest fault activation, the sub-threshold Coulomb stress values suggest that the observed fissure may have resulted from site effects or ground amplification in sedimentary basins as documented by Branner (1915) and Pérez and Aguirre (1988), rather than direct fault activation.

Previous work by Cortés-Aranda et al. (2022), based on Freed (2005), suggests that after a large earthquake, the stress distribution along a receiver fault can lead to its reactivation if the critically stressed fault is located in a region of positive Coulomb failure stress exceeding the triggering threshold. This concept is particularly relevant for structures like the Marga-Marga fault, where, although we lack certainty about its historical activity, this framework helps us better understand how the fault responds to stress parameters induced by different subduction earthquakes. Such understanding would improve our ability to anticipate fault behavior during future events in the same segment.

4.1.3 Limitations and Future Research Directions

While our Coulomb stress analysis produces good results that correlate with historical observations, we acknowledge the need for more robust investigations to fully assess the seismic potential of the Marga-Marga fault. Our current model assumes a fault depth of 10 km, but the true depth extent remains uncertain. As demonstrated by Moreno et al. (2012), stress accumulation patterns can vary significantly with depth, potentially amplifying triggering effects in deeper fault segments.

The high stress values calculated for the 1730 event (approximately 5 bars) could highlight the significant intensity of stress transfer that may have occurred during this large megathrust event. These notably high values, while mechanically plausible, underscore the importance of understanding fault properties beyond Coulomb stress calculations, including frictional and structural characteristics, and loading history that may modulate the fault's response to stress perturbations.

The 2010 Maule earthquake, and subsequent activation of the Pichilemu fault system (Farías et al., 2011) provide an important analog for understanding potential crustal fault responses to large subduction events in Chile in the segment of the Valparaiso region. Following the Maule

earthquake, this sequence demonstrated that crustal faults in Chile can indeed be triggered by subduction events, particularly when stress changes are concentrated on optimally oriented structures.

Future research on the Marga-Marga fault should include:

1. Detailed microseismic monitoring to detect low-magnitude events that may indicate ongoing stress adjustment processes in this segment (for example, see Sippl et al. (2021)).
2. Integration of geodetic data to identify potential aseismic creep or locking behavior that could influence stress accumulation patterns.
3. Trenching studies at key locations along the fault trace to identify evidence of prehistoric ruptures and establish recurrence intervals.
4. Slip distributions of possible events or/and microsismicity in the fault segment.

These approaches would provide a more comprehensive understanding of the fault's seismic potential and its role in the regional stress field, going beyond the limitations of static Coulomb stress modeling alone.

4.1.4 Implications for Seismic Hazard Assessment

Despite the need for further investigation, our results provide valuable input for understanding the potential behavior of the Marga-Marga fault during future large-magnitude subduction earthquakes. The consistent stress loading patterns observed across three historical events suggest that this structure should be considered in regional seismic hazard assessments, particularly given its proximity to densely populated urban areas.

The lessons from the 2010 Maule earthquake and Pichilemu fault activation emphasize that crustal faults can respond to subduction earthquakes with significant triggered seismicity, even when such faults have not shown prominent historical activity. This underscores the importance of identifying and characterizing potentially active crustal structures throughout Chile seismically active regions.

As noted by Ruiz et al. (2014), the traditional focus on subduction hazard in Chile has sometimes overshadowed the potential contribution of crustal faults to seismic hazard. Our analysis of the Marga-Marga fault contributes to addressing this gap by highlighting a specific structure that appears susceptible to triggering from major subduction events and could potentially generate localized strong ground motion affecting the metropolitan areas of Viña del Mar and Valparaíso.

4.2 Conclusion

This research has provided significant insights into the seismic history and potential hazards of Central Chile Valparaiso region through a comprehensive analysis of historical earthquakes and their interaction with the Marga-Marga crustal fault. Our research revealed distinct rupture patterns for three major seismic events: the 1730 megathrust earthquake (Mw 9.1), characterized by extensive shallow rupture along nearly 1000 km of coastline, that may have similar characteristics to the Tohoku-oki 2011 earthquake, where the maximum slip area extended toward the trench; the 1906 Valparaíso earthquake (Mw 8.1), with deeper slip concentrated between 33°-34°S; and the 1985 Algarrobo earthquake (Mw 8.0), featuring intermediate-depth rupture concentrated around 33.5°S.

The stochastic logic-tree approach, combined with historical data on vertical displacements, tsunami inundations, and the calculation of uncertainties between each model, enabled robust characterization of these events despite inherent uncertainties. Our findings detail that following the 1730 earthquake, which was characterized by its extensive rupture and magnitude, a series of smaller and deeper events have occurred from this event to the present day. This pattern creates an opportunity to consider that, given Chile's seismic history, a future event could have similar rupture characteristics and magnitude as the 1730 event in this segment. The observed cyclical pattern—where major events are interspersed with sequences of moderate-magnitude earthquakes—suggests a recurrent seismic regime that merits careful monitoring. Herein lies the importance of generating and reconstructing the slip distributions of these past events to better understand their patterns and compare them with previous works and historical data for confirmation.

Coulomb stress analysis revealed that both the 1730 and 1985 historical earthquakes generated stress changes exceeding the triggering threshold (0.1-0.3 MPa or 1-3 bars; Freed, 2005) along the Marga-Marga fault, while the 1906 earthquake produced positive but sub-threshold stress changes (maximum 0.59 bars). In all cases, normal stress was the dominant mechanism, constituting 100% of the stress contribution despite differing magnitudes, which is mechanically consistent with the normal fault classification used as model input. These consistent loading patterns provide a mechanical explanation for the spatial correlation between the fault trace and historical damage reports, suggesting a persistent coupling between subduction events and this crustal structure. Our comparative analysis of the three historical events yielded a particularly intriguing finding: the 1985 earthquake (Mw 8.0) generated greater stress loading on the Marga-Marga fault than the larger 1906 event (Mw 8.1). This seemingly counterintuitive result highlights that the characteristics of the rupture, specifically depth, location, and directivity, can be more influential than magnitude alone in determining how effectively stress transfers to the crustal structures. The intermediate-depth rupture of the 1985 event, centered precisely at the latitude of the fault, created an optimal stress field for fault activation. This insight enriches our understanding of subduction-crustal fault interactions and demonstrates the necessity of considering detailed rupture geometries when evaluating potential triggered seismicity in complex tectonic environments.

The significant period (nearly 300 years) without a major event comparable to the 1730 earthquake indicates substantial accumulated strain energy in the shallow portions of the subduction interface. This energy accumulation, coupled with the inferred interaction between subduction events and the Marga-Marga fault that we present in this thesis, underscores the region's considerable seismic hazard potential.

This work represents more than just data points and models; it embodies our commitment to understanding the forces that shape this region. This study establishes a solid foundation for more comprehensive seismic hazard assessments in this densely populated region. Future research should focus on detailed microseismic monitoring, geodetic observations, and paleoseismic investigations to better quantify the Marga-Marga fault's seismic potential and its role in the regional stress field, which can be conducted based on the reconstruction of slip patterns for this zone. The integration of crustal fault dynamics into hazard models is essential for developing effective mitigation strategies for the Valparaíso metropolitan area, where the interplay between megathrust events and crustal fault responses could significantly amplify localized seismic hazards, ultimately affecting the communities we all strive to protect.

Bibliography

Javiera Alvarez-Vargas, Ignacia Calisto, Rodrigo Cifuentes-Lobos, Claudio Faccenna, Joaquín Cortés-Aranda, and Rodolfo Araya. Code and data for megathrust earthquake characterization along the central chile gap: Exploring historical earthquakes using the stochastic logic tree approach, 2025. URL https://doi.org/10.5281/zenodo.15206982.

S Barrientos, E Vera, P Alvarado, and Tony Monfret. Crustal seismicity in central chile. *Journal of South American Earth Sciences*, 16(8):759–768, 2004.

Sergio Barrientos and National Seismological Center (CSN) Team. The seismic network of chile. *Seismological Research Letters*, 89(2A):467–474, 2018.

Sergio E Barrientos. Dual seismogenic behavior: the 1985 central chile earthquake. *Geophysical research letters*, 22(24):3541–3544, 1995.

Susan Beck, Sergio Barrientos, Eduardo Kausel, and M Reyes. Source characteristics of historic earthquakes along the central chile subduction askew et alzone. *Journal of South American Earth Sciences*, 11(2):115–129, 1998.

Susan L Bilek and Thorne Lay. Subduction zone megathrust earthquakes. *Geosphere*, 14(4): 1468–1500, 2018.

JC Branner. Bibliografia general de temblores y terremotos: Por f. de montessus de ballore. primera parte: Teorias sismologicas, efectos geologicos de los terremotos, catalogos sismicos mundiales. publicada por la sociedad chilena de historia y geografia. roy. 8°, 115 pages; titles 1-644. segunda parte: Europa septentrionel y central, pp. 117-253; titles 645-1560. santiago de chile, 1915, 1915.

Francisco Bravo, Pablo Koch, Sebastian Riquelme, Mauricio Fuentes, and Jaime Campos. Slip distribution of the 1985 valparaíso earthquake constrained with seismic and deformation data. *Seismological Research Letters*, 90(5):1792–1800, 2019.

Thomas Cahill and Bryan L Isacks. Seismicity and shape of the subducted nazca plate. *Journal of Geophysical Research: Solid Earth*, 97(B12):17503–17529, 1992.

Lauren D Carpenter, Farzad Naeim, Marshall Lew, Nabih F Youssef, Fabian Rojas, G Rodolfo Saragoni, and Macarena Schachter Adaros. Performance of tall buildings in viña del mar in the 27 february 2010 offshore maule, chile earthquake. *The Structural Design of Tall and Special Buildings*, 20(1):17–36, 2011.

María X Urbina Carrasco, Nicolás Gorigoitía Abbott, and Marco Cisternas Vega. Aportes a la historia sísmica de chile: el caso del gran terremoto de 1730. *Anuario de estudios americanos*, 73(2):657–687, 2016.

Matías Carvajal and Alejandra Gubler. The effects on tsunami hazard assessment in chile of assuming earthquake scenarios with spatially uniform slip. *Global Tsunami Science: Past and Future, Volume I*, pages 3693–3702, 2017.

Matías Carvajal, Marco Cisternas, Patricio Catalán, and Nicolas Gorigoitía. Redimensionando el terremoto de 1730 de chile central, mediante evidencias históricas y geológicas del tsunami resultante. In *VIII SLAGF y IV SIAGF. Simposio Latino-Americano de Geografía Física—-Simposio Ibero-Americano de Geografía Física "Riesgos, vulnerabilidades y resiliencia socioambiental para enfrentar los cambios globales", Eje*, pages 1134–1142, 2014.

Matías Carvajal, Marco Cisternas, and PA Catalán. Source of the 1730 chilean earthquake from historical records: Implications for the future tsunami hazard on the coast of metropolitan chile. *Journal of Geophysical Research: Solid Earth*, 122(5):3648–3660, 2017.

Matías Carvajal, Marco Cisternas, Alejandra Gubler, and Diego Muñoz. Tsunamis pasados y futuros en chile central. In *La zona costera en Chile: adaptación y planificación para la resiliencia*, pages 130–149, 2019.

M Celebi. Topographical and geological amplifications determined from strong-motion and aftershock records of the 3 march 1985 chile earthquake. *Bulletin of the Seismological Society of America*, 77(4):1147–1167, 1987.

George L Choy and Stephen H Kirby. Apparent stress, fault maturity and seismic hazard for normal-fault earthquakes at subduction zones. *Geophysical Journal International*, 159(3):991–1012, 2004.

Douglas H Christensen and Larry J Ruff. Rupture process of the march 3, 1985 chilean earthquake. *Geophysical Research Letters*, 13(8):721–724, 1986.

Rodrigo Cifuentes-Lobos, Ignacia Calisto, Breanyn MacInnes, Marcos Moreno, Jorge Quezada, Javiera San Martín, Matías Fernández-Palma, and Cristian Saavedra. A stochastic approach to the characterization of the seismic sources: a potential method for the assessment of sources of historical and paleo tsunami. *Stochastic Environmental Research and Risk Assessment*, pages 1–13, 2023.

Marco Cisternas, Brian F Atwater, Fernando Torrejón, Yuki Sawai, Gonzalo Machuca, Marcelo Lagos, Annaliese Eipert, Cristián Youlton, Ignacio Salgado, Takanobu Kamataki, et al. Predecessors of the giant 1960 chile earthquake. *Nature*, 437(7057):404–407, 2005.

Diana Comte, A Eisenberg, E Lorca, M Pardo, L Ponce, R Saragoni, SK Singh, and G Suárez. The 1985 central chile earthquake: A repeat of previous great earthquakes in the region? *Science*, 233(4762):449–453, 1986.

J Cortés-Aranda, J González, D Molina, L Astudillo-Sotomayor, A Tassara, M Miller, F Álvarez-Amado, R González, and D Bahamondes. Linking upper-plate fault reactivation with the megathrust earthquake cycle: The case of the northern chile outer forearc (19° s–23° s). *Tectonics*, 41(11):e2021TC006956, 2022.

Marcelo Farías, Diana Comte, Steven Roecker, Daniel Carrizo, and Mario Pardo. Crustal extensional faulting triggered by the 2010 chilean earthquake: The pichilemu seismic sequence. *Tectonics*, 30(6), 2011.

Andrew M Freed. Earthquake triggering by static, dynamic, and postseismic stress transfer. *Annu. Rev. Earth Planet. Sci.*, 33(1):335–367, 2005.

Toshiya Fujiwara, Shuichi Kodaira, Tetsuo No, Yuka Kaiho, Narumi Takahashi, and Yoshiyuki Kaneda. The 2011 tohoku-oki earthquake: Displacement reaching the trench axis. *Science*, 334 (6060):1240–1240, 2011.

Yo Fukutani, Anawat Suppasri, and Fumihiko Imamura. Quantitative assessment of epistemic uncertainties in tsunami hazard effects on building risk assessments. *Geosciences*, 8(1):17, 2018.

Paulina Gana, Renate Wall, and Alvaro Gutiérrez. Mapa geológico del área de valparaíso-curacaví, regiones de valparaíso y metropolitana. 1996.

Katsuichiro Goda and Jie Song. Uncertainty modeling and visualization for tsunami hazard and risk mapping: a case study for the 2011 tohoku earthquake. *Stochastic environmental research and risk assessment*, 30:2271–2285, 2016.

Joan Gomberg and Brian Sherrod. Crustal earthquake triggering by modern great earthquakes on subduction zone thrusts. *Journal of Geophysical Research: Solid Earth*, 119(2):1235–1250, 2014.

Juan González, Gabriel González, Rafael Aránguiz, Diego Melgar, Natalia Zamora, Mahesh N Shrivastava, Ranjit Das, Patricio A Catalan, and Rodrigo Cienfuegos. A hybrid deterministic and stochastic approach for tsunami hazard assessment in iquique, chile. *Natural Hazards*, 100: 231–254, 2020.

Kurt Grimme and Leonardo Álvarez. El suelo de fundación de valparaíso y viña del mar: geología del área valparaíso-viña del mar. 1964.

Marc-André Gutscher, Wim Spakman, Harmen Bijwaard, and E Robert Engdahl. Geodynamics of flat subduction: Seismicity and tomographic constraints from the andean margin. *Tectonics*, 19(5):814–833, 2000.

Gavin P Hayes, Ginevra L Moore, Daniel E Portner, Mike Hearne, Hanna Flamme, Maria Furtney, and Gregory M Smoczyk. Slab2, a comprehensive subduction zone geometry model. *Science*, 362(6410):58–61, 2018.

Francisco Hernandez, Pedro Soto, Leonardo Massone, Samantha Salazar, and matias costa. Doble resonancia de edificio con instrumentación sísmica en la cuenca del marga-marga. 10 2023.

Takeshi Iinuma, Mako Ohzono, Yusaku Ohta, and Satoshi Miura. Coseismic slip distribution of the 2011 off the pacific coast of tohoku earthquake (m 9.0) estimated based on gps data—was the asperity in miyagi-oki ruptured? *Earth, planets and space*, 63:643–648, 2011.

Julius Jara-Muñoz, Daniel Melnick, Patricio Zambrano, Andreas Rietbrock, Javiera González, Boris Argandoña, and Manfred R Strecker. Quantifying offshore fore-arc deformation and splay-fault slip using drowned pleistocene shorelines, arauco bay, chile. *Journal of Geophysical Research: Solid Earth*, 122(6):4529–4558, 2017.

Jean M Johnson, Kenji Satake, Sanford R Holdahl, and Jeanne Sauber. The 1964 prince william sound earthquake: Joint inversion of tsunami and geodetic data. *Journal of Geophysical Research: Solid Earth*, 101(B1):523–532, 1996.

Hiroo Kanamori. The diversity of large earthquakes and its implications for hazard mitigation. *Annual Review of Earth and Planetary Sciences*, 42(1):7–26, 2014.

Thorne Lay. A review of the rupture characteristics of the 2011 tohoku-oki mw 9.1 earthquake. *Tectonophysics*, 733:4–36, 2018.

Thorne Lay, Hiroo Kanamori, Charles J Ammon, Keith D Koper, Alexander R Hutko, Lingling Ye, Han Yue, and Teresa M Rushing. Depth-varying rupture properties of subduction zone megathrust faults. *Journal of Geophysical Research: Solid Earth*, 117(B4), 2012.

Randall J LeVeque, Knut Waagan, Frank I González, Donsub Rim, and Guang Lin. Generating random earthquake events for probabilistic tsunami hazard assessment. *Global Tsunami Science: Past and Future, Volume I*, pages 3671–3692, 2017.

Felipe Leyton, Sergio Ruiz, and Sergio A Sepúlveda. Reevaluación del peligro sísmico probabilístico en chile central. *Andean geology*, 37(2):455–472, 2010.

Cinna Lomnitz. Major earthquakes and tsunamis in chile during the period 1535 to 1955. *Geologische Rundschau*, 59:938–960, 1970.

John P Loveless, Richard W Allmendinger, Matthew E Pritchard, and Gabriel González. Normal and reverse faulting driven by the subduction zone earthquake cycle in the northern chilean fore arc. *Tectonics*, 29(2), 2010.

Raúl Madariaga. Sismicidad de chile. *Física de la Tierra*, 10(1):221–258, 1998.

P Martin Mai and Gregory C Beroza. A spatial random field model to characterize complexity in earthquake slip. *Journal of Geophysical Research: Solid Earth*, 107(B11):ESE–10, 2002.

Valentina Maldonado, Martín Contreras, and Daniel Melnick. A comprehensive database of active and potentially-active continental faults in chile at 1: 25,000 scale. *Scientific data*, 8(1):20, 2021.

Carolina Martínez, Rodrigo Hidalgo, Cristián Henríquez, Federico Arenas, Nelson Rangel-Buitrago, and Manuel Contreras-López. La zona costera en chile: adaptación y planificación para la resiliencia. *Instituto de Geografía-Serie Geolibros. Santiago: Ediciones UC*, 2019.

Marianne Metois, C Vigny, and A Socquet. Interseismic coupling, megathrust earthquakes and seismic swarms along the chilean subduction zone (38–18 s). *Pure and Applied Geophysics*, 173: 1431–1449, 2016.

M Moreno, Daniel Melnick, Matthias Rosenau, John Bolte, Juergen Klotz, Helmut Echtler, J Baez, K Bataille, Jun Chen, M Bevis, H. Hase, and O. Oncken. Heterogeneous plate locking in the south–central chile subduction zone: Building up the next great earthquake. *Earth and Planetary Science Letters*, 305(3-4):413–424, 2011.

M Moreno, Daniel Melnick, Matthias Rosenau, J Baez, Jan Klotz, Onno Oncken, Andres Tassara, Jun Chen, K Bataille, M Bevis, et al. Toward understanding tectonic control on the mw 8.8 2010 maule chile earthquake. *Earth and Planetary Science Letters*, 321:152–165, 2012.

Marcos Moreno, Matthias Rosenau, and Onno Oncken. 2010 maule earthquake slip correlates with pre-seismic locking of andean subduction zone. *Nature*, 467(7312):198–202, 2010.

Eleonora Muñoz, S Sepulveda, and Sofía Rebolledo. Nuevos antecedentes sobre la falla marga-marga y sus implicancias en el peligro sísmico. In *XIII Congreso Geológico Chileno*, 2012.

NOAA National Centers for Environmental Information. Significant earthquake information: Chile valparaiso 1730. https://www.ngdc.noaa.gov/hazel/view/hazards/earthquake/event-more-info/1246, n.d. Accessed: [fecha de acceso].

Emile A Okal. A re-evaluation of the great aleutian and chilean earthquakes of 1906 august 17. *Geophysical Journal International*, 161(2):268–282, 2005.

Shinzaburo Ozawa, Takuya Nishimura, Hisashi Suito, Tomokazu Kobayashi, Mikio Tobita, and Tetsuro Imakiire. Coseismic and postseismic slip of the 2011 magnitude-9 tohoku-oki earthquake. *Nature*, 475(7356):373–376, 2011.

Alfredo Palacios Roa. Fuentes para la historia sísmica de chile (1570-1906). *Fuentes para la historia sísmica de Chile (1570-1906*, 2016.

M Pardo, D Comte, and T Monfret. Seismotectonic and stress distribution in the central chile subduction zone. *Journal of South American Earth Sciences*, 15(1):11–22, 2002.

Luis E. Pérez and C. Aguirre. Microzonificación sísmica de la ciudad de viña del mar. Memoria para optar al título de ingeniero civil, Universidad Técnica Federico Santa María, Valparaíso, Chile, 1988.

Belle Philibosian and Aron J Meltzner. Segmentation and supercycles: A catalog of earthquake rupture patterns from the sumatran sunda megathrust and other well-studied faults worldwide. *Quaternary Science Reviews*, 241:106390, 2020.

N Philippi and L Garrido. Recopilación de estudios en relación a la falla marga-marga y su implicancia en el peligro sísmico del plan de viña del mar. 2016.

Tsuneji Rikitake. Recurrence of great earthquakes at subduction zones. *Tectonophysics*, 35(4): 335–362, 1976.

Alfredo Palacios Roa. El gran terremoto de 1730: la experiencia santiaguina frente a la catástrofe. *Temas americanistas*, (22), 2009.

Alfredo Rodríguez Rozas and Cardos Gajardo Cruzat. *La catástrofe del 16 de agosto de 1906 en la república de Chile*. Imprenta, litografía y encuadernación, Barcelona, 1906.

JC Ruegg, A Rudloff, C Vigny, R Madariaga, JB De Chabalier, J Campos, E Kausel, S Barrientos, and D Dimitrov. Interseismic strain accumulation measured by gps in the seismic gap between constitución and concepción in chile. *Physics of the Earth and Planetary Interiors*, 175(1-2): 78–85, 2009.

S Ruiz, M Metois, A Fuenzalida, J Ruiz, F Leyton, R Grandin, C Vigny, R Madariaga, and J Campos. Intense foreshocks and a slow slip event preceded the 2014 iquique m w 8.1 earthquake. *Science*, 345(6201):1165–1169, 2014.

Sergio Ruiz and Raúl Madariaga. Historical and recent large megathrust earthquakes in chile. *Tectonophysics*, 733:37–56, 2018.

Javiera San Martín, Ignacia Calisto, Jorge Quezada, Daniel Stewart, Lisa Ely, Rodrigo Cifuentes-Lobos, and Marcos Moreno. Characterization of historical megathrust earthquake ruptures in central chile using logic tree analysis. *Natural Hazards*, 120(6):5411–5427, 2024.

Isabel Santibáñez, José Cembrano, Tiaren García-Pérez, Carlos Costa, Gonzalo Yáñez, Carlos Marquardt, Gloria Arancibia, and Gabriel González. Crustal faults in the chilean andes: geological constraints and seismic potential. *Andean Geology*, 46(1):32–65, 2019.

Rodolfo Saragoni, Paulina González, and Marcelo Fresard. *Analisis de los Acelerogramas del Terremoto del 3 de Marzo de 1985*. Universidad de Chile, Facultad de Ciencias Físicas y Matemáticas ..., 1985.

Kenji Satake and Mohammad Heidarzadeh. A review of source models of the 2015 illapel, chile earthquake and insights from tsunami data. *The Chile-2015 (Illapel) Earthquake and Tsunami*, pages 1–9, 2017.

Mark Simons, Sarah E Minson, Anthony Sladen, Francisco Ortega, Junle Jiang, Susan E Owen, Lingsen Meng, Jean-Paul Ampuero, Shengji Wei, Risheng Chu, et al. The 2011 magnitude 9.0 tohoku-oki earthquake: Mosaicking the megathrust from seconds to centuries. *science*, 332 (6036):1421–1425, 2011.

Christian Sippl, Marcos Moreno, and Roberto Benavente. Microseismicity appears to outline highly coupled regions on the central chile megathrust. *Journal of Geophysical Research: Solid Earth*, 126(11):e2021JB022252, 2021.

William Spence. Slab pull and the seismotectonics of subducting lithosphere. *Reviews of Geophysics*, 25(1):55–69, 1987.

Daniel Stewart. Historical tsunamis in the concepcion bay, as seen in the reconstructed flood levels from the colonial city of concepcion (penco), chile (1570-1835). *Revista de Historia*, 2(26): 97–127, 2019.

Daniel M Stewart. Recalibrando el terremoto del 8 de julio de 1730 en valparaíso, chile: dando contexto histórico a las fuentes primarias. *Revista de historia (Concepción)*, 27(2):103–141, 2020.

Hisashi Suito and Jeffrey T Freymueller. A viscoelastic and afterslip postseismic deformation model for the 1964 alaska earthquake. *Journal of Geophysical Research: Solid Earth*, 114(B11), 2009.

Yuichiro Tanioka, Tomohiro Kususose, S Kathiroli, Yuichi Nishimura, Sin-Iti Iwasaki, and Kenji Satake. Rupture process of the 2004 great sumatra-andaman earthquake estimated from tsunami waveforms. *Earth, planets and space*, 58(2):203–209, 2006.

R Thorson. La falla geológica marga-marga, viña del mar-chile. *Universidad Técnica Federico Santa María, Departamento de Obras Civiles, Valparaíso*, 1999.

F Tilmann, Y Zhang, M Moreno, Joachim Saul, Felix Eckelmann, M Palo, Z Deng, Andrey Babeyko, Kejie Chen, Juan Carlos Báez, B. Schurr, R. Wang, and T. Dahm. The 2015 illapel earthquake, central chile: A type case for a characteristic earthquake? *Geophysical Research Letters*, 43(2):574–583, 2016.

Shinji Toda, Ross S Stein, Volkan Sevilgen, and Jian Lin. Coulomb 3.3 graphic-rich deformation and stress-change software for earthquake, tectonic, and volcano research and teaching—user guide. *US Geological Survey open-file report*, 1060(2011):63, 2011.

Agustin Udias, Elisa Buforn, and Raul Madariaga. Large chilean earthquakes and tsunamis of 1730 and 1751: new analysis of historical data. In *EGU General Assembly Conference Abstracts*, pages EGU2013–1079, 2013.

María X. Urbina-Carrasco, Nicolás Gorigoitía-Abbott, and Marco Cisternas-Vega. Contributions to the Chile's seismic history: the case of the great earthquake of 1730. *Anuario de Estudios Americanos*, 73(2):657–687, 2016. doi: 10.3989/aeamer.2016.2.11.

Jaime Valenzuela Márquez. Relaciones jesuitas del terremoto de 1730: Santiago, valparaíso y concepción. *Cuadernos de historia (Santiago)*, (37):195–224, 2012.

Gabriel Villavicencio and Gonzalo Suazo. Geotechnical characterization of viña del mar for areas where buildings were affected by mega-earthquakes in central chile. *Earthquake Spectra*, 38(4): 2521–2547, 2022.

R Von Huene, J Corvalán, ER Flueh, K Hinz, J Korstgard, CR Ranero, and W Weinrebe. Tectonic control of the subducting juan fernández ridge on the andean margin near valparaiso, chile. *Tectonics*, 16(3):474–488, 1997.

Jianjun Wang, Caijun Xu, Jeffrey T Freymueller, Yangmao Wen, and Zhuohui Xiao. Autocoulomb: An automated configurable program to calculate coulomb stress changes on receiver faults with any orientation and its application to the 2020 m w 7.8 simeonof island, alaska, earthquake. *Seismological Society of America*, 92(4):2591–2609, 2021.

Huihui Weng and Jean-Paul Ampuero. The dynamics of elongated earthquake ruptures. *Journal of Geophysical Research: Solid Earth*, 124(8):8584–8610, 2019.

Sharon L Wood, James K Wight, and Jack P Moehle. The 1985 chile earthquake: observations on earthquake-resistant construction in viña del mar. *Civil Engineering Studies SRS-532*, 1987.

Gonzalo A Yáñez, César R Ranero, Roland von Huene, and Juan Díaz. Magnetic anomaly interpretation across the southern central andes (32–34 s): The role of the juan fernández ridge in the late tertiary evolution of the margin. *Journal of Geophysical Research: Solid Earth*, 106 (B4):6325–6345, 2001.

Yong-Fei Zheng and Zi-Fu Zhao. Introduction to the structures and processes of subduction zones. *Journal of Asian Earth Sciences*, 145:1–15, 2017.

X Zhou, G Cambiotti, W Sun, and R Sabadini. The coseismic slip distribution of a shallow subduction fault constrained by prior information: the example of 2011 tohoku (m w 9.0) megathrust earthquake. *Geophysical Journal International*, 199(2):981–995, 2014.